AD NUMBER

AD866199

LIMITATION CHANGES

TO:

Approved for public release; distribution is unlimited. Document partially illegible.

FROM:

Distribution authorized to U.S. Gov't. agencies and their contractors; Critical Technology; DEC 1969. Other requests shall be referred to U.S. Army Aviation Materiel Laboratories, Eustis, VA 23604. Document partially illegible. This document contains export-controlled technical data.

AUTHORITY

USAAMRDL ltr, 23 Jun 1971

AD

USAAVLABS TECHNICAL REPORT 69-86

FAILURE ANALYSIS OF INITIALLY IMPERFECT, AXIALLY COMPRESSED, ORTHOTROPIC, SANDWICH AND ECCENTRICALLY STIFFENED, CIRCULAR CYLINDRICAL SHELLS

By

D. L. Wesenberg

J. Mayers

December 1969

U. S. ARMY AVIATION MATERIEL LABORATORIES
FORT EUSTIS, VIRGINIA

CONTRACT DAAJ02-68-C-0035

STANFORD UNIVERSITY

STANFORD, CALIFORNIA

79

DISCLAIMER NOTICE

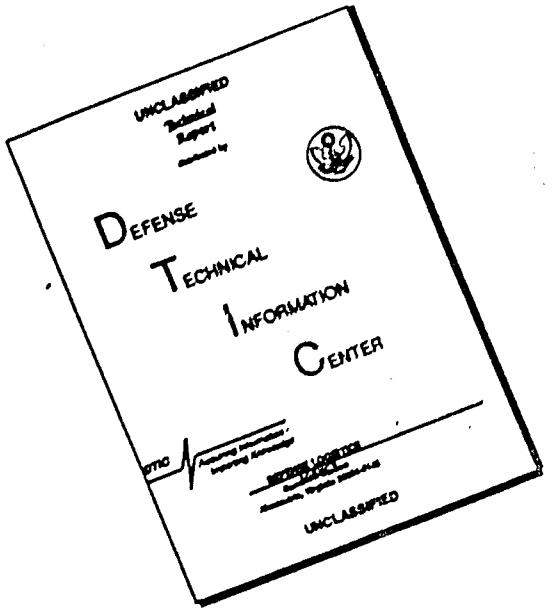

THIS DOCUMENT IS BEST QUALITY AVAILABLE. THE COPY FURNISHED TO DTIC CONTAINED A SIGNIFICANT NUMBER OF PAGES WHICH DO NOT REPRODUCE LEGIBLY.

Disclaimers

The findings in this report are not to be construed as an official Department of the Army position unless so designated by other authorized documents.

When Government drawings, specifications, or other data are used for any purpose other than in connection with a definitely related Government procurement operation, the United States Government thereby incurs no responsibility nor any obligation whatsoever; and the fact that the Government may have formulated, furnished, or in any way supplied the said drawings, specifications, or other data is not to be regarded by implication or otherwise as in any manner licensing the holder or any other person or corporation, or conveying any rights or permission, to manufacture, use, or sell any patented invention that may in any way be related thereto.

Disposition Instructions

Destroy this report when no longer needed. Do not return it to the originator.

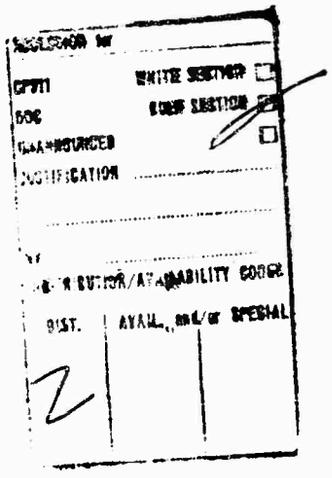

DEPARTMENT OF THE ARMY
HEADQUARTERS US ARMY AVIATION MATERIEL LABORATORIES
FORT EUSTIS, VIRGINIA 23604

This program was carried out under Contract DAAJ02-68-C-0035 with Stanford University.

The data contained in this report are the result of research conducted in the failure analysis of initially imperfect, axially compressed, sandwich and eccentrically stiffened, circular cylindrical shells. The maximum strength analysis is based on Reissner's variational principle, von Kármán-Donnell kinematics, and deformation theory of plasticity.

The report has been reviewed by the U.S. Army Aviation Materiel Laboratories and is considered to be technically sound. It is published for the exchange of information and the stimulation of future research.

Task 1F162204A17002
Contract DAAJ02-68-C-0035
USAAVLABS Technical Report 69-86
December 1969

FAILURE ANALYSIS OF INITIALLY IMPERFECT, AXIALLY COMPRESSED, ORTHOTROPIC, SANDWICH AND ECCENTRICALLY STIFFENED, CIRCULAR CYLINDRICAL SHELLS

By

D. L. Wesenberg and J. Mayers

Prepared by
Stanford University
Stanford, California

for

U.S. ARMY AVIATION MATERIEL LABORATORIES
FORT EUSTIS, VIRGINIA

ABSTRACT

The maximum strength analysis of initially imperfect, axially compressed, orthotropic, sandwich and eccentrically stiffened, circular cylindrical shells has been developed through the use of Reissner's variational principle, von Kármán-Donnell kinematics, and a deformation theory of plasticity. For a given material and for the special cases of isotropic sandwich cylinders and conventional cylinders with eccentrically located longitudinal stiffeners, the results of the analysis reflect significant reductions in load-carrying capability in the range of "effective" radius-to-thickness ratios of practical interest.

FOREWORD

The work reported herein constitutes a portion of a continuing effort being undertaken at Stanford University for the U. S. Army Aviation Materiel Laboratories under Contract DAAJ02-68-C-0035 (Task 1F162204A17002) to establish accurate theoretical prediction capability for the static and dynamic behavior of aircraft structural components utilizing both conventional and unconventional materials. Predecessor contracts supported investigations which led, in part, to the results presented in references 4, 15, 16, 17, 19, and 21.

TABLE OF CONTENTS

LIST OF ILLUSTRATIONS

LIST OF SYMBOLS

A	cross-sectional area of stiffener, $in.^2$
A_{ij}	nondimensional direct stress coefficient
a_{ij}, b_{ij}	nondimensional bending stress coefficients
C	nondimensional eccentricity constant
D	bending stiffness of isotropic cylinder, $D = \frac{Et^3}{12(1-\nu^2)}$, lb-in.
D_x, D_y	bending stiffnesses of orthotropic cylinder in x- and y-directions, respectively, lb-in.
D_{xy}	twisting stiffness of orthotropic cylinder, lb-in.
D_q	transverse shear stiffness of isotropic, sandwich cylinder $D_q = G_c t_c$, lb/in.
d	stringer spacing, in.
d_{ij}	nondimensional bending stress coefficient
E	Young's modulus, psi
E_x, E_y	extensional stiffnesses of orthotropic cylinder in x- and y-directions, respectively, lb/in.
e	unit end shortening, in./in.
e_{cl_o}	classical unit end shortening of sandwich cylinder with infinitely rigid core in./in.
F'	stress energy density, psi
F_{ij}	nondimensional strain parameter, in./in.
G	shear modulus, psi
G_{xy}	midsurface shear stiffness of orthotropic cylinder, lb/in.
G_c	shear modulus for isotropic core of sandwich cylinder, psi

G_{xz}, G_{yz}	shear moduli for orthotropic core of sandwich cylinder, psi
H_{ij}	nondimensional strain parameter, in./in.
h	distance separating the faces of two-element, isotropic cylinder, in.
h_x, h_y	distances separating the faces of two-element, orthotropic cylinder in x- and y-directions, respectively, in.
h_{xy}	fictitious weighted average of h_x and h_y, in.
I	moment of inertia of stiffener about its centroid, $in.^4$
J	torsional constant for stiffener, $in.^4$
K	nondimensional Ramberg-Osgood material constant
k_i	extensional stiffness parameter of orthotropically stiffened cylinder, lb/in.
L	length of cylinder, in.
ℓ	ring spacing, in.
M_x, M_y	bending moments per unit length in x- and y-directions, respectively, lb
M_{xy}	twisting moment per unit length, lb
m	number of axial waves
N	nondimensional Ramberg-Osgood material constant
n	number of circumferential waves
R	radius of cylinder, in.
$\bar{R}$	nondimensional extensional stiffness ratio for ring, $\bar{R} = \frac{E_r A_r}{Et\ell}$
$\bar{S}$	nondimensional extensional stiffness ratio for stringer, $\bar{S} = \frac{E_s A_s}{Etd}$

s'_x, s'_y, s'_{xy}, s'	nondimensional extensional stiffness parameters of orthotropic cylinder
$s''_x, s''_y, s''_{xy}, s''$	nondimensional bending stiffness parameters of orthotropic cylinder
t	thickness of homogeneous, isotropic cylinder, in.
t_c	thickness of core of sandwich cylinder, in.
t_f	thickness of face sheet of sandwich cylinder, in.
$\bar{t}$	effective thickness of orthotropically stiffened cylinder, $\bar{t} = \frac{A_s}{d} + t$, in.
U''	Reissner functional, lb-in.
V	volume of two-element cylinder, $V = 4\pi t_f LR$, in.^{3}
u,v,w	displacements of point on middle surface of cylinder in x-, y-, and z-directions, respectively, in.
w_o	initial deviation of midsurface displacement in radial direction, in.
x,y	cylinder coordinates, in.
Z	nondimensional curvature parameter, $Z = \frac{L^2\sqrt{1-\nu^2}}{Rt}$
z	cylinder coordinate, in.
$\bar{z}$	distance from centroid of stiffener to middle surface of cylinder, in.
α	nondimensional wave parameter, $\alpha = \frac{m\pi R}{L}$
β	nondimensional wave aspect ratio, $\beta = \frac{nL}{m\pi R}$
$\Gamma_{x_{ij}}, \Gamma_{y_{ij}}$	nondimensional transverse shear coefficients
Γ	nondimensional transverse shear parameter, $\Gamma = (\pi^2 E t_f h)/[2(1-\nu^2)D_q R]$
γ_{xy}	total shear strain in the xy-plane, in./in.
γ'_{xy}	shear strain at middle surface, in./in.
γ''_{xy}	shear strain due to twisting, in./in.

γ_{xz}, γ_{yz}	total shear strains in xz- and yz-planes, respectively, in./in.
$\Delta_r, \Delta_s, \Delta_{rs}, \bar{\Delta}$	nondimensional stiffened cylinder parameters (defined in equations (76))
Δ	nondimensional imperfection parameter, $\Delta = \xi_{11_o}/\bar{t}$
δ	nondimensional imperfection parameter, $\delta = \xi_{11_o}/h$
ε_{eff}	effective strain, in./in.
ϵ_x, ϵ_y	total strains in x- and y-directions, respectively, in./in.
ϵ_x', ϵ_y'	strains due to bending in x- and y-directions, respectively, in./in.
$\epsilon_x'', \epsilon_y''$	strains due to bending in x- and y-directions, respectively, in./in.
η	nondimensional wave parameter, $\eta = n^2 \frac{h}{R}$
$\bar{\eta}$	nondimensional wave parameter, $\bar{\eta} = n^2 \frac{\bar{t}}{R}$
κ_x, κ_y	changes in curvature of the shell midsurface, 1/in.
κ_{xy}	change in twist of shell midsurface, 1/in.
λ_x, λ_y	buckle half wave lengths in x- and y-directions, respectively, in.
μ	nondimensional buckle aspect ratio
μ_x, μ_y	nondimensional Poisson's ratios for extension of orthotropic cylinder in x- and y-directions, respectively
ν	nondimensional Poisson's ratio for isotropic cylinder
ν_x, ν_y	nondimensional Poisson's ratios for bending of orthotropic cylinder in x- and y-directions, respectively
ξ_{ij}	nondimensional displacement coefficient

ξ_{ij_o}	nondimensional imperfection amplitude coefficient
σ	average compressive stress, psi
σ_{cl}	classical buckling stress, psi
σ_{cl_o}	classical stress of sandwich cylinder with infinitely rigid core, psi
σ_{eff}	effective stress, psi
σ_x, σ_y	total stresses in x- and y-directions, respectively, psi
σ'_x, σ'_y	average direct stresses in x- and y-directions, respectively, psi
σ''_x, σ''_y	bending stresses in x- and y-directions, respectively, psi
τ_{xy}	total shear stress in xy-plane, psi
τ'_{xy}	average shear stress in xy-plane, psi
τ''_{xy}	shear stress due to bending, psi
τ_{xz}, τ_{yz}	transverse shear stresses in xz- and yz-planes, respectively, psi

SUBSCRIPTS

b	denotes bottom face of two-element model
f	denotes face sheet
i,j	integers
o	denotes radial imperfection
r,s	denote properties of rings and stringers, respectively
ST	denotes stiffened shell
TE	denotes two-element model
t	denotes top face of two-element model
x,y,z	denote longitudinal, circumferential, and radial directions, respectively

INTRODUCTION

The challenge of designing lightweight structures with high strength and stiffness for aerospace applications has not yet been met even though significant advances have been made in vehicle capability. One of the fundamental problems precluding true structural optimization is that the most common structural element for resisting compression loadings, the thin shell, can be analyzed for design purposes only on a semi-empirical basis. The history of the 40-year-old enigmatic thin-shell instability problem through 1967 is given in several recent survey papers by Hoff[1,2] and Stein[3]. The basic reasons established for the discrepancy between prediction and actual performance of thin shells in compression are the effects of prebuckling deformations, initial imperfections in shell geometry, and boundary conditions. Interestingly, except for noting the theoretical limitations of the linear-elastic theories surveyed, neither author discusses nor assesses the quantitative effects of inelastic deformations on the maximum strength (initial buckling load) of cylindrical shells in axial compression. The extreme importance of inelastic deformations in determining the maximum strength of such shells has been brought out recently by Mayers and Wesenberg[4]. They determined that, in the range of shell radius-to-thickness ratios of practical interest, significant maximum-strength reductions are obtained relative to predictions based upon any theory restricted to linear-elastic material behavior. Since thin shells for resisting compression loads appear in aerospace structures in either stiffened or sandwich rather than pure monocoque form, the "effective" radius-to-thickness ratios are in the range 50-250. The low ratio is mentioned specifically by Hoff[1]. For the range 50-250, it is apparent that the effects of initial imperfections, the main contributor to theory-experiment discrepancies in thin, unstiffened shells (radius-to-thickness ratios > 250), must be minimized and the effects of inelastic deformations maximized in establishing maximum strength. This maximum-strength problem, with inelastic deformations considered, is not to be confused with the plastic buckling of shells treated, for example, by Lee[5] and Batterman[6]. Such shells are

prone to be inefficient compared with shells which, if devoid of initial imperfections, would buckle at the classical buckling level of the linear theory arrived at independently by Timoshenko[7], Lorenz[8], and Southwell[9] about 60 years ago.

Now, in view of the results of reported compression tests on large-scale sandwich and stiffened shells (references 10, 11, 12) in the radius-to-thickness-ratio range 45-220, maximum calculated stresses indicate the presence of inelastic deformations at maximum load. Therefore, in view of the main conclusion of Mayers and Wesenberg[4] and experimental evidence, the present study has been undertaken to determine the influence of inelastic deformations on the maximum load of initially imperfect, axially compressed, circular cylindrical shells of stiffened and sandwich construction. For the latter, considerations of the face-dimpling and face-wrinkling modes of instability have not been considered.

The present study follows the approach used in reference 4 and differs from it only in the provision of appropriate mechanisms for describing orthotropic sandwich and stiffened shells (including eccentricity effects). That is, the investigation uses a modified from of Reissner's variational principle[13] in conjunction with von Kármán-Donnell shell theory and a deformation theory of plasticity. Reissner's variational principle not only permits the selection of the stresses independent of the displacements, but also facilitates the incorporation of inelastic effects into the analysis. Confidence in the inelastic analysis based on Reissner's principle has been established in reference 4 by comparing a special case of a purely elastic solution with that obtained by Kempner[14] through use of the minimum total potential energy principle. Similar procedures were followed by Mayers et al.[15,16] with respect to both plates and circular cylindrical shells. With confidence previously established, maximum-strength, load-shortening curves have been obtained for sandwich shells (isotropic cores) and axially stiffened shells (eccentricity effects included) of several different materials. Because of the significant material dependence of these curves, it is reasonable to conclude that inelastic deformations must be included in determining

the maximum strength of sandwich and stiffened cylindrical shells in axial compression. Although only specific illustrations have been given for the two types of shells, the procedure is general and may be followed for any set of geometric and material shell parameters corresponding to sandwich shells with orthotropic cores and orthotropic shells with eccentrically located stiffeners.

GENERAL THEORY

STATEMENT OF PROBLEM AND BASIC ASSUMPTIONS

The general problem studied is the maximum strength of orthotropic sandwich and stiffened (eccentricity effects included) circular cylindrical shells in axial compression. The solutions are obtained through the use of a modified version of the Reissner principle, the von Kármán-Donnell strain-displacement relations, and a deformation theory of plasticity. Since no unloading in the nonlinear, inelastic range occurred in the monocoque shell analysis of reference 4, it is assumed that the terms nonlinear elastic and inelastic can be used interchangeably. For the sandwich shells, no provision is incorporated to allow for the face-wrinkling and face-dimpling modes of instability.

The model used to describe stiffened and sandwich cylindrical shells is shown in Figure 1 and comprises a two-element cross section and core of finite transverse shear stiffness in both the xz- and yz-planes, respectively. The effectiveness of this model was demonstrated by Mayers and Chu[17] in their maximum-load predictions for sandwich plates. The two-element section with the core rigid in shear has been employed by Mayers et al.[4,15-19] in their extensive maximum-strength studies of plates and cylindrical shells to avoid the complexity, due to inelastic effects, of integrating a nonlinear stress distribution through the thickness.

The strain-displacement equations used in the present analysis are those of von Kármán-Donnell for shallow, initially imperfect, circular cylindrical shells. Since the magnitudes of both deflections and rotations are small as determined by Mayers and Wesenberg[4], the use of the von Kármán-Donnell strain-displacement equations is justified.

BASIC EQUATIONS

The von Kármán-Donnell strain-displacement relations, modified to include the effects of initial imperfections, are well known (for example, see reference 4); they are given here as

$$\varepsilon'_x = u_{,x} + \frac{1}{2} w_{,x}^2 + w_{,x} w_{o,x}$$

$$\varepsilon'_y = v_{,y} + \frac{1}{2} w_{,y}^2 + w_{,y} w_{o,y} - \frac{w}{R} \qquad (1)$$

$$\gamma'_{xy} = u_{,y} + v_{,x} + w_{,x} w_{,y} + w_{o,x} w_{,y} + w_{o,y} w_{,x}$$

The curvature-displacement equations have been modified to include the effects of transverse shear (for example, see reference 17) and are given by

$$\kappa_x = -w_{,xx} + \gamma_{xz,x}$$

$$\kappa_y = -w_{,yy} + \gamma_{yz,y} \qquad (2)$$

$$\kappa_{xy} = -w_{,xy} + \frac{1}{2} \gamma_{xz,y} + \frac{1}{2} \gamma_{yz,x}$$

The total strains are then

$$\varepsilon_x = \varepsilon'_x + z \kappa_x$$

$$\varepsilon_y = \varepsilon'_y + z \kappa_y \qquad (3)$$

$$\gamma_{xy} = \gamma'_{xy} + 2z \kappa_{xy}$$

VARIATIONAL PRINCIPLE

Because of its proven success in determining the maximum strength of plates and shells (see references 4, 15, and 17), the Reissner principle is selected for application in this problem. For prescribed surface displacements (controlled end shortening), the Reissner functional is simply

$$U'' = \iiint_V [\sigma_x \varepsilon_x + \sigma_y \varepsilon_y + \tau_{xy} \gamma_{xy} + \tau_{yz} \gamma_{zy} + \tau_{xz} \gamma_{xz} - F'] \, dV \qquad (4)$$

where F' is the stress energy density. F' is a function of the stresses such that the strains are related to the stresses by the relationships

$$\epsilon_x = \frac{\partial F'}{\partial \sigma_x}, \epsilon_y = \frac{\partial F'}{\partial \sigma_y}, \gamma_{xy} = \frac{\partial F'}{\partial \tau_{xy}}, \gamma_{xz} = \frac{\partial F'}{\partial \tau_{xz}}, \gamma_{yz} = \frac{\partial F'}{\partial \tau_{yz}} \tag{5}$$

The functional given by equation (4) is utilized in the indirect variational approach to develop Euler equation boundary conditions for both orthotropic sandwich and stiffened cylindrical shells in Appendixes I and II, respectively. For problems involving linear-elastic material behavior, F' becomes the complementary energy density. As shown in references 4, 15, and 18 for a nonlinear elastic material, F' is given by

$$F' = \int_0^{\sigma_{eff}} \epsilon_{eff} \, d\sigma_{eff} \tag{6}$$

The relationship between ϵ_{eff} and σ_{eff} is given by the Ramberg-Osgood[20] three-parameter representation of a uniaxial stress-strain curve in the form

$$\epsilon_{eff} = \frac{\sigma_{eff}}{E} + K\left(\frac{\sigma_{eff}}{E}\right)^N \tag{7}$$

where K and N are material constants and depend on a given material. Upon substitution of equations (6) and (7) into equation (4) and subsequent integration, the Reissner functional becomes

$$U'' = \iiint \left\{ \sigma_x \epsilon_x + \sigma_y \epsilon_y + \tau_{xy}\gamma_{xy} + \tau_{xz}\gamma_{xz} + \tau_{yz}\gamma_{yz} - \left[\frac{\sigma_{eff}^2}{2E} + \frac{KE}{N+1}\left(\frac{\sigma_{eff}}{E}\right)^{N+1} \right] \right\} dV \tag{8}$$

Consideration of purely elastic core behavior, and integration over the cross section results in the expression

$$\begin{aligned} \frac{U''}{EV} = \iint_0^1 \int_0^1 \Bigg\{ & \frac{\sigma'_x}{E}\epsilon'_x + \frac{\sigma'_y}{E}\epsilon'_y + \frac{\tau'_{xy}}{E}\gamma'_{xy} + \frac{\sigma''_x}{E}\epsilon''_x \\ & + \frac{\sigma''_y}{E}\epsilon''_y + \frac{\tau''_{xy}}{E}\gamma''_{xy} + \frac{t_c}{2t_f}\left[\frac{\tau_{xz}}{E}\gamma_{xz} + \frac{\tau_{yz}}{E}\gamma_{yz}\right] \\ & - \frac{t_c}{4t_f}\left[\frac{E}{G_{xz}}\left(\frac{\tau_{xz}}{E}\right)^2 + \frac{E}{G_{yz}}\left(\frac{\tau_{yz}}{E}\right)^2\right] \\ & - \frac{1}{4}\left[\left(\frac{\sigma_{eff}}{E}\right)_t^2 + \left(\frac{\sigma_{eff}}{E}\right)_b^2\right] - \frac{1}{2}\frac{K}{(N+1)}\left[\left(\frac{\sigma_{eff}}{E}\right)_t^{N+1} + \left(\frac{\sigma_{eff}}{E}\right)_b^{N+1}\right] \Bigg\} d\omega d\epsilon \end{aligned} \tag{9}$$

where $\omega = x/L$, $\epsilon = y/2\pi R$, and $V = \pi t_f LR$. The primed and double-primed quantities refer to the midsurface and bending contributions, respectively. The subscripts t and b refer to the top and bottom faces, respectively, of the model cross section.

METHOD OF SOLUTION

ISOTROPIC SANDWICH, CIRCULAR CYLINDRICAL SHELLS

Although the general theory has been established for sandwich shells with orthotropic cores, the application is made herein to the special case of an isotropic core. Thus, the following simplifications can be made:

$$G_{xz} = G_{yz} = G_c = \frac{\tau_{xz}}{\gamma_{xz}} = \frac{\tau_{yz}}{\gamma_{yz}}$$

$$G_{xy} = \frac{E}{2(1+\nu)} \tag{10}$$

It can be verified also that

$$\frac{1}{4}\left[\left(\frac{\sigma_{eff}}{E}\right)_t^2 + \left(\frac{\sigma_{eff}}{E}\right)_b^2\right] = \frac{1}{2}\left[\left(\frac{\sigma'_x}{E}\right)^2 + \left(\frac{\sigma'_y}{E}\right)^2 - 2\nu\left(\frac{\sigma'_x}{E}\right)\left(\frac{\sigma'_y}{E}\right) + 2(1+\nu)\left(\frac{\tau'_{xy}}{E}\right)^2 + \left(\frac{\sigma''_x}{E}\right)^2 + \left(\frac{\sigma''_y}{E}\right)^2 - 2\nu\left(\frac{\sigma''_x}{E}\right)\left(\frac{\sigma''_y}{E}\right) + 2(1+\nu)\left(\frac{\tau''_{xy}}{E}\right)^2\right] \tag{11}$$

Substitution of equations (10) and (11) into equation (9) with Poisson's ratio taken as 0.5 (incompressible material assumption justified *a posteriori* in RESULTS AND DISCUSSION) leads to the result

$$\frac{U''}{EV} = \int_0^1\int_0^1 \left\{\frac{\sigma'_x}{E}\epsilon'_x + \frac{\sigma'_y}{E}\epsilon'_y + \frac{\tau'_{xy}}{E}\gamma'_{xy} + \frac{\sigma''_x}{E}\epsilon''_x + \frac{\sigma''_y}{E}\epsilon''_y + \frac{\tau''_{xy}}{E}\gamma''_{xy} + \frac{1}{4}\frac{G_c t_c}{E t_f}\left(\gamma_{xz}^2 + \gamma_{yz}^2\right)\right.$$

$$\left. - \frac{1}{2}\left[\left(\frac{\sigma'_x}{E}\right)^2 + \left(\frac{\sigma'_y}{E}\right)^2 - \left(\frac{\sigma'_x}{E}\right)\left(\frac{\sigma'_y}{E}\right) + 3\left(\frac{\tau'_{xy}}{E}\right)^2 + \left(\frac{\sigma''_x}{E}\right)^2 + \left(\frac{\sigma''_y}{E}\right)^2 - \left(\frac{\sigma''_x}{E}\right)\left(\frac{\sigma''_y}{E}\right) + 3\left(\frac{\tau''_{xy}}{E}\right)^2\right]\right\}$$

$$- \frac{1}{2} \frac{K}{(N+1)} \left| \left(\frac{\sigma_{eff}}{E} \right)_t^{N+1} + \left(\frac{\sigma_{eff}}{E} \right)_b^{N+1} \right| \int d\varepsilon \tag{12}$$

Displacement, Stress, and Shear Strain Formulations

The displacements from the initial shape are selected to be

$$w = h(\xi_{00} + \xi_{11} \cos \frac{\pi x}{\lambda_x} \cos \frac{\pi y}{\lambda_y} + \xi_{20} \cos \frac{2\pi x}{\lambda_x} + \xi_{02} \cos \frac{2\pi y}{\lambda_y} \tag{13}$$

$$u = -\varepsilon x \tag{14}$$

$$v = 0 \tag{15}$$

where ε is the prescribed unit end shortening. These displacements are the same functions as those used in reference 4 with the radial displacement identical to that of Kempner[14]. The rationale underlying the use of expressions for u and v involving no free parameters has been demonstrated and clearly justified in references 4 and 15. This significant simplification of the expressions for the midsurface displacements permits the inplane equilibrium equations in the x- and y-directions to be satisfied independently of the magnitudes of the free stress coefficients.

From the findings of Mayers and Wrenn[21] and Tennyson and Welles[22], as pointed out in reference 4, an initial radial imperfection shape to which a cylindrical shell is particularly sensitive is

$$w_o = h\left| \xi_{11_o} \cos \frac{\pi x}{\lambda_x} \cos \frac{\pi y}{\lambda_y} + \xi_{20_o} \cos \frac{2\pi x}{\lambda_x} \right| \tag{16}$$

The midsurface stresses can be expressed in the form

$$\frac{\sigma'_x}{E} = - \left| \frac{\sigma}{E} + A_{11} \cos \frac{\pi x}{\lambda_x} \cos \frac{\pi y}{\lambda_y} + 4A_{22} \cos \frac{2\pi y}{\lambda_x} \cos \frac{2\pi y}{\lambda_y} + 9A_{13} \cos \frac{\pi x}{\lambda_x} \cos \frac{3\pi y}{\lambda_y} + A_{31} \cos \frac{3\pi x}{\lambda_x} \cos \frac{\pi y}{\lambda_y} + 4A_{02} \cos \frac{2\pi y}{\lambda_y} \right| \tag{17}$$

$$\frac{\tau'_{xy}}{E} = -\left| A_{11} \sin \frac{\pi x}{\lambda_x} \sin \frac{\pi y}{\lambda_y} + 4A_{22} \sin \frac{2\pi x}{\lambda_x} \sin \frac{2\pi y}{\lambda_y} \right.$$

$$+ 3A_{13} \sin \frac{\pi x}{\lambda_x} \sin \frac{3\pi y}{\lambda_y} + 3A_{31} \sin \frac{3\pi x}{\lambda_x} \sin \frac{\pi y}{\lambda_y} \Big| \tag{18}$$

$$\frac{\sigma'_y}{E} = -\mu^2 \Big| A_{11} \cos \frac{\pi x}{\lambda_x} \cos \frac{\pi y}{\lambda_y} + 4A_{22} \cos \frac{2\pi x}{\lambda_x} \cos \frac{2\pi y}{\lambda_y}$$

$$+ A_{13} \cos \frac{\pi x}{\lambda_x} \cos \frac{3\pi y}{\lambda_y} + 9A_{31} \cos \frac{3\pi x}{\lambda_x} \cos \frac{\pi y}{\lambda_y} + 4A_{20} \cos \frac{2\pi x}{\lambda_x} \Big| \tag{19}$$

The equivalence of the coefficients in $\frac{\sigma'_x}{E}$, $\frac{\sigma'_y}{E}$, and $\frac{\tau'_{xy}}{E}$ is established from direct satisfaction of the inplane equilibrium equations in view of the fact that the u and v displacements involve no free paramet s.

The bending stresses are written as

$$\frac{\sigma''_x}{E} = a_{11} \cos \frac{\pi x}{\lambda_x} \cos \frac{\pi y}{\lambda_y} + a_{20} \cos \frac{2\pi x}{\lambda_x} + a_{02} \cos \frac{2\pi y}{\lambda_y} \tag{20}$$

$$\frac{\sigma''_y}{E} = \mu^2 \left[b_{11} \cos \frac{\pi x}{\lambda_x} \cos \frac{\pi y}{\lambda_y} + b_{20} \cos \frac{2\pi x}{\lambda_x} + b_{02} \cos \frac{2\pi y}{\lambda_y} \right] \tag{21}$$

$$\frac{\tau''_{xy}}{E} = \mu \left[d_{11} \sin \frac{\pi x}{\lambda_x} \sin \frac{\pi y}{\lambda_y} \right] \tag{22}$$

The form of the shear strains in the xz- and yz-planes are taken to be compatible with $w_{,x}$ and $w_{,y}$ respectively. Both expressions are then written in the form

$$\gamma_{xz} = \Gamma_{x_{11}} \sin \frac{\pi x}{\lambda_x} \cos \frac{\pi y}{\lambda_y} + \Gamma_{x_{20}} \sin \frac{2\pi x}{\lambda_x} \tag{23}$$

$$\gamma_{yz} = \Gamma_{y_{11}} \cos \frac{\pi x}{\lambda_x} \sin \frac{\pi y}{\lambda_y} + \Gamma_{y_{02}} \sin \frac{2\pi y}{\lambda_y} \tag{24}$$

Elastic Problem

The von Kármán-Donnell strain-displacement relations, modified to include initial radial deformations and transverse shear effects (see Appendix I), are substituted into equation (12) to give

$$\frac{U''}{EV} = \int_0^1 \int_0^1 \left\{ \frac{\sigma'_x}{E} \left[u_{,x} + \frac{1}{2} w_{,x}^2 + w_{,x} w_{o,x} \right] + \frac{\sigma'_y}{E} \left[v_{,y} + \frac{1}{2} w_{,y}^2 \right.\right.$$

$$\left. + w_{,y} w_{o,y} - \frac{w}{R} \right] + \frac{\tau'_{xy}}{E} \left[v_{,x} + u_{,y} + w_{,x} w_{,y} + w_{,x} w_{o,y} \right.$$

$$\left. + w_{,y} w_{o,x} \right] + \frac{\sigma''_x}{E} \frac{h}{2} \left[w_{,xx} - \gamma_{xz,x} \right] + \frac{\sigma''_y}{E} \frac{h}{2} \left[w_{,yy} - \gamma_{yz,y} \right]$$

$$+ \frac{\tau''_{xy}}{E} h \left[w_{,xy} - \frac{1}{2} \left(\gamma_{xz,y} + \gamma_{yz,x} \right) \right] + \frac{1}{4} \frac{G_c t_c}{E t_f} \left(\gamma_{xz}^2 + \gamma_{yz}^2 \right)$$

$$- \frac{1}{2} \left[\left(\frac{\sigma'_x}{E} \right)^2 + \left(\frac{\sigma'_y}{E} \right)^2 - \left(\frac{\sigma'_x}{E} \right) \left(\frac{\sigma'_y}{E} \right) + 3 \left(\frac{\tau'_{xy}}{E} \right)^2 \right]$$

$$+ \left(\frac{\sigma''_x}{E} \right)^2 + \left(\frac{\sigma''_y}{E} \right)^2 - \left(\frac{\sigma''_x}{E} \right) \left(\frac{\sigma''_y}{E} \right) + 3 \left(\frac{\tau''_{xy}}{E} \right)^2 \Bigg]$$

$$- \frac{1}{2} \frac{K}{(N+1)} \left[\left(\frac{\sigma_{eff}}{E} \right)_t^{N+1} + \left(\frac{\sigma_{eff}}{E} \right)_b^{N+1} \right] \Bigg\} dx dz \qquad (25)$$

In consideration of linear-elastic behavior, the bending stresses can be related to the curvatures through Hooke's law, thus modifying the Reissner functional of equation (12). This procedure is followed successfully and justified in references 4, 15, 16, and 17. After setting $K = 0$ (linear elastic material), equation (25) is rewritten as

$$\frac{U''}{EV} = \int_0^1 \int_0^1 \left\{ \frac{\sigma'_x}{E} \left[u_{,x} + \frac{1}{2} w_{,x}^2 + w_{,x} w_{o,x} \right] + \frac{\sigma'_y}{E} \left[v_{,y} + \frac{1}{2} w_{,y}^2 \right.\right.$$

$$\left. + w_{,y} w_{o,y} - \frac{w}{R} \right] + \frac{\tau'_{xy}}{E} \left[v_{,x} + u_{,y} + w_{,x} w_{,y} + w_{o,x} w_{,y} \right.$$

$$\left. + w_{o,y} w_{,x} \right] + \frac{\sigma''_x}{E} \frac{h}{2} \left[w_{,xx} - \gamma_{xz,x} \right] + \frac{\sigma''_y}{E} \left[w_{,yy} - \gamma_{yz,y} \right]$$

$$+ \frac{\tau''_{xy}}{E} h \left[w_{,xy} - \frac{1}{2} \left(\gamma_{xz,y} + \gamma_{yz,x} \right) \right] + \frac{1}{4} \frac{G_c t_c}{E t_f} \left(\gamma_{xz}^2 + \gamma_{yz}^2 \right)$$

$$
- \frac{1}{2} \left[\left(\frac{\sigma'_x}{E} \right)^2 + \left(\frac{\sigma'_y}{E} \right)^2 - \left(\frac{\sigma'_x}{E} \right) \left(\frac{\sigma'_y}{E} \right) + 3 \left(\frac{\tau'_{xy}}{E} \right)^2 \right]
$$

$$
+ \frac{h}{6}^2 \left[\left(w_{,xx} - \gamma_{xz,x} \right)^2 + \left(w_{,yy} - \gamma_{yz,y} \right)^2 \right.
$$

$$
\left. + \left(w_{,xx} - \gamma_{xz,x} \right) \left(w_{,yy} - \gamma_{yz,y} \right) + \left(w_{,xy} - \frac{1}{2} \gamma_{xz,y} - \frac{1}{2} \gamma_{yz,x} \right)^2 \right] \} \, dx \, dz \tag{26}
$$

This modified form of the Reissner functional leaves only the displacements and midsurface stresses to be determined by the variational procedure. The all-elastic, load-shortening curves are established by seeking a stationary value of the Reissner functional in equation (26) with respect to the free parameters ξ_{ij}, A_{ij}, $\Gamma_{x_{ij}}$, $\Gamma_{y_{ij}}$, and σ/E (see Appendix III). The resulting set of equations is reducible to four equations in the four unknowns σ/E, ξ_{11}, ξ_{20}, and ξ_{02}. These equations are then used to construct the elastic, imperfection- and shear parameter-dependent, load-shortening curves shown in Figure 2 for representative values of the buckle wave parameters μ, η, and δ and the core transverse shear stiffness parameter Γ.

Inelastic Problem

Equation (25), consisting of 17 free parameters, can now be utilized for the inelastic problem. The additional parameters over the four required for the elastic solution appear because the bending stresses require seven additional parameters. Neither these seven additional free coefficients a_{11}, a_{20}, a_{02}, b_{11}, b_{20}, b_{02}, and d_{11} nor the six midsurface stress components A_{11}, A_{22}, A_{13}, A_{31}, A_{20}, and A_{02} can be eliminated in terms of the ξ_{11}, ξ_{20}, ξ_{02}, and σ/E because of the highly nonlinear inelastic contribution to the Reissner functional. As a result, the extrema of equation (25) are found with respect to the 17 unknowns by analytic minimization of the Reissner functional and subsequent numerical solution of the resulting nonlinear algebraic equations. A (R/h) - dependent, load-shortening curve is obtained and presented in Figure 3 for a 2024-T3 aluminum sandwich cylinder

with an isotropic core. The uniaxial stress-strain curve of the face sheet material is shown in Figure 4.

ORTHOTROPICALLY STIFFENED CIRCULAR CYLINDRICAL SHELLS

A stiffened, circular cylindrical shell is represented by a two-element model with a core that is infinitely rigid in shear (see Figure 1). The model is allowed the freedom of variable inplane and bending stiffnesses to account for the orthotropic effects of stringers and rings in the longitudinal and circumferential directions, respectively. The general Reissner functional, represented by equation (8), with transverse shear effects neglected is then integrated over the thickness of the model to obtain

$$\frac{U''}{EV} = \int_0^1 \int_0^1 \left\{ \frac{\sigma'_x}{E}\epsilon'_x + \frac{\sigma'_y}{E}\epsilon'_y + \frac{\tau'_{xy}}{E}\gamma'_{xy} + \frac{\sigma''_x}{E}\epsilon''_x + \frac{\sigma''_y}{E}\epsilon''_y + \frac{\tau''_{xy}}{E}\gamma''_{xy} - \frac{1}{4}\left[\left(\frac{\sigma_{eff}}{E}\right)^2_t + \left(\frac{\sigma_{eff}}{E}\right)^2_b\right] - \frac{1}{2}\frac{K}{(N+1)}\left[\left(\frac{\sigma_{eff}}{E}\right)^{N+1}_t + \left(\frac{\sigma_{eff}}{E}\right)^{N+1}_b\right]\right\} d\xi\, d\eta \tag{27}$$

The effective stress in both top and bottom faces, modified to include variable stiffnesses in the x- and y-directions, respectively, is written in the form

$$\sigma^2_{eff_{t,b}} = \left[\frac{\sigma'_x}{\sqrt{s'_x}} \pm \frac{\sigma''_x}{\sqrt{s''_x}}\right]^2 + \left[\frac{\sigma'_y}{\sqrt{s'_y}} \pm \frac{\sigma''_y}{\sqrt{s''_y}}\right]^2 - \left[\frac{\sigma'_x}{\sqrt{s'}} \pm \frac{\sigma''_x}{\sqrt{s''}}\right]\left[\frac{\sigma'_y}{\sqrt{s'}} \pm \frac{\sigma''_y}{\sqrt{s''}}\right] + 3\left[\frac{\tau'_{xy}}{\sqrt{s'_{xy}}} \pm \frac{\tau''_{xy}}{\sqrt{s''_{xy}}}\right]^2 \tag{28}$$

where

$$s'_x = \frac{E_x}{2t_f E}$$

$$s'_y = \frac{E_y}{2t_f E} \tag{29}$$

$$s' = \frac{\left(\frac{E_x}{2t_f E}\right)\left(\frac{E_x}{2t_f E}\right)}{\mu_x \frac{E_y}{2t_f E} + \mu_y \frac{E_y}{2t_f E}}$$

$$s'_{xy} = \frac{3G_{xy}}{2t_f E}$$

$$s''_x = 1 \tag{29}$$

$$s''_y = 1$$

$$s'' = \frac{D_x D_y}{\nu_x D_y + \nu_y D_x}$$

$$s''_{xy} = \frac{3}{2\left(1 + \frac{\nu_x}{2} + \frac{\nu_y}{2}\right)}$$

For an isotropic, two-element model, equations (29) reduce to

$$s'_x = s'_y = s''_x = s''_y = 1$$

$$s' = s'' = \frac{1}{2\nu} \tag{30}$$

$$s'_{xy} = s''_{xy} = \frac{3}{2(1+\nu)}$$

and σ^2_{eff}, in turn, becomes

$$\sigma^2_{eff_{t,b}} = (\sigma'_x \pm \sigma''_x)^2 + (\sigma'_y \pm \sigma''_y)^2 - (\sigma'_x \pm \sigma''_x)(\sigma'_y \pm \sigma''_y) + 3(\tau'_{xy} \pm \tau''_{xy})^2 \tag{31}$$

Hence, the above expression is now identical to that used in references 4, 15, 16, 18, and 19 for isotropic plates and shells. Now, substitution of equation (28) into equation (27) leads to the following result applicable to orthotropic two-element media undergoing nonlinear-elastic deformations:

$$\frac{U''}{EV} = \iint_{0\,0}^{1,1} \Bigg\{ \frac{\sigma'_x}{E}\,\epsilon'_x + \frac{\sigma'_y}{E}\,\epsilon'_y + \frac{\tau'_{xy}}{E}\,\gamma'_{xy} + \frac{\sigma''_x}{E}\,\epsilon''_x + \frac{\sigma''_y}{E}\,\epsilon''_y + \frac{\tau''_{xy}}{E}\,\gamma''_{xy} - \frac{1}{2}\Bigg[\frac{1}{s'_x}\left(\frac{\sigma'_x}{E}\right)^2 + \frac{1}{s'_x}\left(\frac{\sigma'_y}{E}\right)^2 - \frac{1}{s'}\left(\frac{\sigma'_x}{E}\right)\left(\frac{\sigma'_y}{E}\right) + \frac{3}{s'_{xy}}\left(\frac{\tau'_{xy}}{E}\right)^2 + \frac{1}{s''_x}\left(\frac{\sigma''_x}{E}\right)^2 + \frac{1}{s''_y}\left(\frac{\sigma''_y}{E}\right)^2 - \frac{1}{s''}\left(\frac{\sigma''_x}{E}\right)\left(\frac{\sigma''_y}{E}\right) + \frac{3}{s''_{xy}}\left(\frac{\tau''_{xy}}{E}\right)^2\Bigg] - \frac{1}{2}\,\frac{K}{(N+1)}\left[\left(\frac{\sigma_{eff}}{E}\right)_t^{N+1} + \left(\frac{\sigma_{eff}}{E}\right)_b^{N+1}\right]\Bigg\}\,d\omega\,d\epsilon \tag{32}$$

Correlation of Stiffness Parameters

In reference 4, the thickness t of the homogeneous, isotropic, circular cylindrical shell is related to the distance h separating the two faces of the two-element model by equating the classical buckling stress of the homogeneous, isotropic cylinder to that of the two-element cylinder. For the orthotropically stiffened shell, a similar procedure is followed whereby the classical buckling stresses of the stiffened shell (see reference 23) and orthotropic, two-element model are equated to establish expressions relating the bending and midsurface stiffnesses of the stiffened shell to those of the orthotropic, two-element model (see Appendix IV). The resulting relationships correlating the stiffness parameters are derived in Appendix IV, first on the basis of zero stiffener eccentricity effects and then with eccentricity effects included. For the former case, the correspondence of stiffness parameters is

$$\frac{D_x/2t_f}{1-\nu_x\nu_y} = \frac{D}{t}\left[1 + \frac{E_s I_s}{dD}\right]$$

$$\frac{D_y/2t_f}{1-\nu_x\nu_y} = \frac{D}{t}\left[1 + \frac{E_r I_r}{\ell D}\right] \tag{33}$$

$$D_{xy}/2t_f = \frac{D}{t}\left[1 - \frac{\nu_x}{2} - \frac{\nu_y}{2} + \frac{1}{2}\left(\frac{G_s J_s}{dD} + \frac{G_r J_r}{\ell D}\right) - \frac{1}{2}\left(\nu_y \frac{E_s I_s}{dD} + \nu_x \frac{E_r I_r}{\ell D}\right)\right]$$

$$\frac{E_x}{2t_f E} = \frac{k_1}{k_4} = s'_x$$

$$\frac{E_y}{2t_f E} = \frac{k_1}{k_2} = s'_y \tag{34}$$

$$\frac{G_{xy}}{2t_f E} = \frac{k_1}{k_3+\mu_y k_2+\mu_x k_4} = \frac{s'_{xy}}{3}$$

For an isotropic, two-element model, the bending and twisting stiffnesses are related to the distance h separating the two faces and written in the form

$$D_x = \frac{Et_f h^2}{2}$$

$$D_y = \frac{Et_f h^2}{2} \tag{35}$$

$$D_{xy} = \frac{Et_f h^2}{2(1+\nu)}$$

On the other hand, for an orthotropic, two-element model, the bending

stiffnesses must be related to h_x and h_y, the distances separating the faces normal to the x- and y-axes, respectively, and h_{xy}, a fictitious weighted average of h_x and h_y. These h's are then related to the bending and twisting stiffnesses by

$$D_x = \frac{Et_f h_x^2}{2}$$

$$D_y = \frac{Et_f h_y^2}{2} \qquad (36)$$

$$D_{xy} = \frac{Et_f h_{xy}^2}{2\left(1 + \frac{\nu_x}{2} + \frac{\nu_y}{2}\right)}$$

Substitution of equation (36) into equation (33) leads finally to the set of relations

$$\left(\frac{h_x}{\bar{t}}\right)^2 = \frac{1}{3}\left(\frac{1-\nu_x\nu_y}{1-\nu^2}\right)\left(\frac{t}{\bar{t}}\right)^3\left[1 + \frac{E_s I_s}{dD}\right]$$

$$\left(\frac{h_y}{\bar{t}}\right)^2 = \frac{1}{3}\left(\frac{1-\nu_x\nu_y}{1-\nu^2}\right)\left(\frac{t}{\bar{t}}\right)^3\left[1 + \frac{E_r I_r}{\ell D}\right] \qquad (37)$$

$$\left(\frac{h_{xy}}{\bar{t}}\right)^2 = \frac{1}{3}\left(\frac{1 + \frac{\nu_x}{2} + \frac{\nu_y}{2}}{1 - \nu^2}\right)\left(\frac{t}{\bar{t}}\right)^3\left[1 - \frac{\nu_x}{2} - \frac{\nu_y}{2} + \frac{1}{2}\left(\frac{G_s J_s}{dD} + \frac{G_r J_r}{\ell D}\right)\right.$$

$$\left. - \frac{1}{2}\left(\nu_y \frac{E_s I_s}{dD} + \nu_x \frac{E_t I_r}{\ell D}\right)\right]$$

Equations (37) are reducible to those of the isotropic, two-element model used in reference 4 by introducing the simplifications

$$h_x = h_y = h_{xy} = h$$

$$t = \bar{t}$$

and by eliminating all quantities subscripted with either s or r. The resulting expression is simply $(h/t)^2 = 1/3$, which is identical to the expression derived, for example, in reference 4.

The first-order effects of stiffener eccentricity are established in the detailed development given in Appendix IV. The fundamental bending stiffnesses appearing in equations (33) and (83) are modified approximately to give

$$\frac{D_x/2t_f}{1-\nu_x\nu_y} = \frac{Et^3}{12\bar{t}(1-\nu^2)}\left[1+\frac{E_sI_s}{dD}\right] - C\frac{\bar{S}t^2E\left(\frac{t}{\bar{t}}\right)}{1+(1-\nu^2)\bar{S}}\left(\frac{\bar{z}_s}{R}\right)$$

$$\frac{D_y/2t_f}{1-\nu_x\nu_y} = \frac{Et^3}{12\bar{t}(1-\nu^2)}\left[1+\frac{E_rI_r}{\ell D}\right] - C\frac{\bar{R}t^2E\left(\frac{t}{\bar{t}}\right)}{1+(1-\nu^2)\bar{R}}\left(\frac{\bar{z}_r}{R}\right) \qquad (38)$$

$$D_{xy}/2t_f = \frac{Et^3}{12\bar{t}(1-\nu^2)}\left[1-\frac{\nu_x}{2}-\frac{\nu_y}{2}+\frac{1}{2}\left(\frac{G_sJ_s}{dD}+\frac{G_rJ_r}{\ell D}\right)\right.$$

$$-\frac{1}{2}\left(\nu_y\frac{E_sI_s}{dD}+\nu_x\frac{E_rI_r}{\ell D}\right) + \frac{\nu_y}{2}\left[\frac{C\bar{S}t^2E\left(\frac{t}{\bar{t}}\right)}{1+(1-\nu^2)\bar{S}}\left(\frac{\bar{z}_s}{R}\right)\right]$$

$$\left.+\frac{\nu_x}{2}\left[\frac{C\bar{R}t^2E\left(\frac{t}{\bar{t}}\right)}{1+(1-\nu^2)\bar{R}}\left(\frac{\bar{z}_r}{R}\right)\right] - \frac{1}{2}\left[\frac{C(1-\nu^2)\bar{R}\,\bar{S}t^2E\left(\frac{t}{\bar{t}}\right)}{2+2(1-\nu)(\bar{R}+\bar{S})+2\bar{R}\bar{S}(1-\nu^2)(1+\nu)}\left(\frac{\bar{z}_r}{R}+\frac{\bar{z}_s}{R}\right)\right]\right]$$

where $\bar{z}_s$ and $\bar{z}_r$ are the distances from the shell median surface to the centroids of the axial and circumferential stiffeners, respectively, and C is a nondimensional eccentricity constant.

Substitution of equations (36) into equations (38) yields

$$\left(\frac{h_x}{\bar{t}}\right)^2 = \frac{1}{3}\left(\frac{1-\nu_x\nu_y}{1-\nu^2}\right)\left(\frac{t}{\bar{t}}\right)^3\left[1+\frac{E_sI_s}{dD}\right] - C\,\frac{4\bar{S}(1-\nu_x\nu_y)}{1+(1-\nu^2)\bar{S}}\left(\frac{t}{\bar{t}}\right)^3\left(\frac{\bar{z}_s}{R}\right)$$

$$\left(\frac{h_y}{\bar{t}}\right)^2 = \frac{1}{3}\left(\frac{1-\nu_x\nu_y}{1-\nu^2}\right)\left(\frac{t}{\bar{t}}\right)^3\left[1+\frac{E_rI_r}{\ell D}\right] - C\,\frac{4\bar{R}(1-\nu_x\nu_y)}{1+(1-\nu^2)\bar{R}}\left(\frac{t}{\bar{t}}\right)^3\left(\frac{\bar{z}_r}{R}\right)$$

$$\left(\frac{h_{xy}}{\bar{t}}\right)^2 = \frac{1}{3}\left(\frac{1+\frac{\nu_x}{2}+\frac{\nu_y}{2}}{1-\nu^2}\right)\left(\frac{t}{\bar{t}}\right)^3\left[1-\frac{\nu_x}{2}-\frac{\nu_y}{2}+\frac{1}{2}\left(\frac{G_sJ_s}{dD}+\frac{G_rJ_r}{\ell D}\right)\right. \tag{39}$$

$$\left.-\frac{1}{2}\left(\nu_y\frac{E_sI_s}{dD}+\nu_x\frac{E_rI_r}{\ell D}\right)\right]+2\nu_y\left(1+\frac{\nu_x}{2}+\frac{\nu_y}{2}\right)\left[\frac{C\bar{S}}{1+(1-\nu^2)\bar{S}}\left(\frac{t}{\bar{t}}\right)^3\left(\frac{\bar{z}_s}{R}\right)\right]$$

$$+2\nu_x\left(1+\frac{\nu_x}{2}+\frac{\nu_y}{2}\right)\left[\frac{C\bar{R}}{1+(1-\nu^2)\bar{R}}\left(\frac{t}{\bar{t}}\right)^3\left(\frac{\bar{z}_r}{R}\right)\right]$$

$$-2\left(1+\frac{\nu_x}{2}+\frac{\nu_y}{2}\right)\left[\frac{C(1-\nu^2)\bar{R}\,\bar{S}\left(\frac{t}{\bar{t}}\right)^3}{2+2(1+\nu)(\bar{R}+\bar{S})+2\bar{R}\,\bar{S}(1-\nu^2)(1+\nu)}\left(\frac{\bar{z}_r}{R}+\frac{\bar{z}_s}{R}\right)\right]$$

Displacement and Stress Formulations

Equations (13) through (22) are used to represent the displacement and stress distributions; they are of the same form as those selected by Kempner[14]. However, the nondimensionalizing factor h in equations (13) and (16) has been replaced with the effective thickness, $\bar{t}$, of the stiffened circular cylinder. These two equations are then rewritten as

$$w = \bar{t}\left(\xi_{00}+\xi_{11}\cos\frac{\pi x}{\lambda_x}\cos\frac{\pi y}{\lambda_y}+\xi_{20}\cos\frac{2\pi x}{\lambda_x}+\xi_{02}\cos\frac{2\pi y}{\lambda_y}\right) \tag{40}$$

$$w_o = \bar{t}\left(\xi_{11_o}\cos\frac{\pi x}{\lambda_x}\cos\frac{\pi y}{\lambda_y}+\xi_{20_o}\cos\frac{2\pi x}{\lambda_x}\right) \tag{41}$$

Elastic Problem

The von Kármán-Donnell, strain-displacement relations presented in Appendix II for the initially imperfect, orthotropic, two-element model are substituted in equation (32) to give

$$\frac{U''}{EV} = \int_0^1\int_0^1\left\{\frac{\sigma'_x}{E}\left[u_{,x}+\frac{1}{2}w_{,x}^2+w_{,x}w_{o,x}\right]+\frac{\sigma'_x}{E}\left[v_{,y}+\frac{1}{2}w_{,y}^2+w_{,y}w_{o,y}\right.\right.$$

$$- \frac{w}{R}\Bigg] + \frac{\tau'_{xy}}{E}\left[v_{,x} + u_{,y} + w_{,x}w_{,y} + w_{,x}w_{o,y} + w_{,y}w_{o,x}\right]$$

$$+ \frac{\sigma''_x}{E}\left[\frac{h_x}{2}w_{,xx}\right] + \frac{\sigma''_y}{E}\left[\frac{h_y}{2}w_{,yy}\right] + \frac{\tau''_{xy}}{E}\left[h_{xy}w_{,xy}\right]$$

$$- \frac{1}{2}\left[\frac{1}{s'_x}\left(\frac{\sigma'_x}{E}\right)^2 + \frac{1}{s'_y}\left(\frac{\sigma'_y}{E}\right)^2 - \frac{1}{s'}\left(\frac{\sigma'_x}{E}\right)\left(\frac{\sigma'_y}{E}\right) + \frac{3}{s'_{xy}}\left(\frac{\tau'_{xy}}{E}\right)^2 + \frac{1}{s''_x}\left(\frac{\sigma''_x}{E}\right)^2 + \frac{1}{s''_y}\left(\frac{\sigma''_y}{E}\right)^2\right.$$

$$\left. - \frac{1}{s''}\left(\frac{\sigma''_x}{E}\right)\left(\frac{\sigma''_y}{E}\right) + \frac{3}{s''_{xy}}\left(\frac{\tau''_{xy}}{E}\right)^2\right] - \frac{1}{2}\frac{K}{(N+1)}\left[\left(\frac{\sigma_{eff}}{E}\right)_t^{N+1} + \left(\frac{\sigma_{eff}}{E}\right)_b^{N+1}\right]\Bigg\} dxdz \tag{42}$$

For linear-elastic material behavior, K is set equal to zero, and the procedure of relating the bending stresses to the curvatures through Hooke's law can be used again, as in the case of the isotropic sandwich cylinder. Equation (42) is then rewritten in the form

$$\frac{U'''}{EV} = \int_0^1\int_0^1 \Bigg\{\frac{\sigma'_x}{E}\left[u_{,x} + \frac{1}{2}w_{,x}^2 + w_{,x}w_{o,x}\right] + \frac{\sigma'_y}{E}\left[v_{,y} + \frac{1}{2}w_{,y}^2 + w_{,y}w_{o,y} - \frac{w}{R}\right]$$

$$+ \frac{\tau'_{xy}}{E}\left[v_{,x} + u_{,y} + w_{,x}w_{,y} + w_{,x}w_{o,y} + w_{o,x}w_{,y}\right]$$

$$+ \frac{\sigma''_x}{E}\left[\frac{h_x}{2}w_{,xx}\right] + \frac{\sigma''_y}{E}\left[\frac{h_y}{2}w_{,yy}\right] + \frac{\tau''_{xy}}{E}\left[h_{xy}w_{,xy}\right]$$

$$- \frac{1}{2}\left[\frac{1}{s'_x}\left(\frac{\sigma'_x}{E}\right)^2 + \frac{1}{s'_y}\left(\frac{\sigma'_y}{E}\right)^2 - \frac{1}{s'}\left(\frac{\sigma'_x}{E}\right)\left(\frac{\sigma'_y}{E}\right) + \frac{3}{s'_{xy}}\left(\frac{\tau'_{xy}}{E}\right)^2\right]$$

$$+ \frac{1}{8(1-\nu_x\nu_y)}\left[h_x^2 w_{,xx}^2 + h_y^2 w_{,yy}^2 + (\nu_y h_x^2 + \nu_x h_y^2)\, w_{,xx}w_{,yy}\right.$$

$$\left. + \frac{2(1-\nu_x\nu_y)}{\left(1 + \frac{\nu_x}{2} + \frac{\nu_y}{2}\right)} h_{xy}^2 w_{,xy}^2\right]\Bigg\} dxdz \tag{43}$$

Equation (43) now contains only displacements and midsurface stresses as variationally dependent quantities. A stationary value of equation (43) is then sought with respect to the free parameters ξ_{ij}, A_{ij}, and σ/E

(see Appendix V); the resulting set of nonlinear algebraic equations is reducible to four equations in the unknowns ξ_{11}, ξ_{20}, ξ_{02}, and σ/E. These four equations are then used to construct the all-elastic, load-end shortening curves presented in Figure 5 for representative values of the buckle wave parameters μ, $\bar{\eta}$, and λ and the orthotropic shell stiffness parameters s'_x, s'_y, s'_{xy}, s', s''_x, s''_y, s''_{xy}, and s''.

Inelastic Problem

In the inelastic problem, equation (42) must be used . As pointed out in the sandwich shell maximum-strength analysis of the present work and in the conventional shell maximum-strength analysis of reference 4, the resulting number of free parameters is 17. A stationary value of equation (42) is sought with respect to ξ_{ij}, A_{ij}, a_{ij}, b_{ij}, d_{11}, and σ/E. Maximum-strength, material-dependent, load-shortening curves are obtained and presented in Figure 6 for 2024-T3 aluminum and stainless steel(1/2 hard). The stress-strain curve for the latter is shown in Figure 7. Values of the buckle wave parameters and the stiffness parameters are the same as those used in the elastic analysis.

RESULTS AND DISCUSSION

The maximum strength of initially imperfect, axially compressed, isotropic sandwich and orthotropic stiffened shells (eccentricity effects included) has been studied through the use of a modified form of Reissner's variational principle, the von Kármán-Donnell stain-displacement relations, and a deformation theory of plasticity. Maximum-strength, material-dependent, load-shortening curves have been obtained for stainless steel and 2024-T3 aluminum cylinders. The results are compared with the load-shortening curves obtained for both sandwich and stiffened circular cylindrical shells when the materials remain linearly elastic.

In conducting the numerical analyses involving inelastic deformations, Poisson's ratios ν, ν_x, and μ_x have each been assigned the value 0.5. Trial computations, in which these Poisson's ratios were varied between 0.3 and 0.5, indicated that the incompressible-material assumption (that is, Poisson's ratios equal to 0.5) relative to the direction of loading led to negligible changes in the results based on varying values of ν, ν_x, and μ_x. Poisson's ratios μ_y and ν_y have been calculated from the reciprocal relations $\mu_y = E_y \mu_x / E_x$ and $\nu_y = D_y \nu_x / D_x$ to ensure symmetry in the orthotropic material constant's matrix.

CIRCULAR CYLINDRICAL SANDWICH SHELLS

The effects of transverse shear and inelastic deformations on the maximum strength of circular cylindrical sandwich shells with isotropic cores have been established in this analysis. Considerations of the face-wrinkling and face-dimpling instability modes have been neglected since the interest herein has been aimed at the bending and buckling in general instability.

Based on all-elastic behavior, transverse shear effects markedly reduce the maximum load of a cylindrical sandwich shell, as shown in Figure 2. This trend is consistent with the classical results presented in reference 24. For $\delta = 0.02$ (a reasonable imperfection amplitude for an "effectively" thick sandwich cylinder), the uppermost curve represents the all-elastic, load-shortening curve for an isotropic sandwich cylinder

with a rigid core, $\Gamma = 0$. The curve for $\Gamma = 1$ represents a sandwich cylinder with finite tranverse shear stiffness of the core. The particular value of the shear stiffness parameter is representative of the weak-core materials used in practice. It is noted that for $\Gamma = 1$, the reduction in maximum load from that obtained for the sandwich cylinder with a rigid core is 6%; thus, for a larger value of Γ (weaker core), the reduction in maximum load would be substantially greater. A similar trend was obtained by Mayers and Chu[17] in their maximum load analysis of isotropic sandwich plates.

Inelastic effects are incorporated into the analysis by introducing actual stress-strain curves. In the case of 2024-T3 aluminum, the uniaxial stress-strain curve is shown in Figure 4. As a result, maximum-strength, (R/h) - dependent, load-shortening curves are obtained and presented in Figure 3. The upper curves represent all-elastic behavior for infinite ($\Gamma = 0$) and finite ($\Gamma = 1$) transverse shear stiffnesses, respectively. The lower curves show the effects of inelastic behavior on two 2024-T3 aluminum sandwich cylinders of (R/h)= 200 with $\Gamma = 0$ and $\Gamma = 1$, respectively. As can be seen, the maximum load is reduced 6% by introducing finite tranverse shear ($\Gamma = 1$) and is reduced an additional 14% by including the effects of inelastic behavior in the face sheets. It can be noted also that for a rigid core ($\Gamma = 0$), the reduction in load-carrying capability, due to inelastic deformations, is 16%. However, as mentioned above for a core of finite transverse shear ($\Gamma = 1$), the maximum load was reduced 14% due to inelastic behavior. It might be concluded, therefore, that plasticity affects a rigid-core, isotropic sandwich cylinder to a greater degree than one with finite transverse shear stiffness; this trend was noted by Mayers and Chu[17] in their maximum-strength analysis of isotropic sandwich plates. This phenomenon in both sandwich plates and cylinders is attributed to the fact that the finite transverse shear permits stress relief across each buckle, causing a lower effective strain and, consequently, less reduction in maximum load due to inelastic deformations. However, from the standpoint of inelastic deformations alone, this isotropic sandwich shell of 2024-T3 aluminum reflects not only (R/h) - dependence of the load-

shortening curve for a sufficiently low (R/h) ratio (the same effect established for conventional shells in reference 4), but a significant reduction in maximum strength.

ECCENTRICALLY STIFFENED, CIRCULAR CYLINDRICAL SHELLS

The maximum strength of initially imperfect, axially compressed, eccentrically stiffened, circular cylindrical shells has been obtained for material properties corresponding to stainless steel (1/2 hard) and 2024-T3 aluminum.

The results of a purely elastic analysis, presented in Figure 5, reflect load-shortening curves for integral, longitudinally stiffened, circular cylindrical shells. The integrally stiffened shell cross section, shown in Figure 5, is identical in geometry to that used by Card and Jones[12] in their studies on the buckling of eccentrically stiffened cylinders. The values of the buckle wave parameters, namely, $\mu = 0.5$ and $\bar{\eta} = 0.25$, have been selected to correspond with those of experiment (see reference 12). A reasonable value of the imperfection parameter, $\Delta = 0.5$, was selected; and the value of the eccentricity constant, $C = 60$, was adjusted to yield an accurate representation of the effects of eccentricity on the maximum load of both outside and inside, longitudinally stiffened, cylindrical shells (see reference 12). The upper and lower curves in Figure 5 correspond to externally and internally stiffened cylinders, respectively. Both types possess the same integral stiffener cross section. It can be noted that the externally stiffened shell carries 38% more axial load than its internally stiffened counterpart, a result which is consistent with those obtained in references 12 and 23. However, this may not always be the case, due to the findings of Hutchinson and Amazigo[25]. They show that for certain ranges of the curvature parameter, $Z = \frac{L^2}{R^2}\sqrt{1-\nu^2}$, an outside stiffened shell is much more imperfection sensitive than one with inside stiffening. However, in the present analysis, the stiffened shell configuration is in the large Z range and, therefore, is out of the region in which an outside stiffened shell should be any more imperfection sensitive than one with inside stiffening.

The effects of inelastic behavior are displayed in Figure 6 by using the stress-strain curve of stainless steel (1/2 hard), shown in Figure 7, and perturbing from the free elastic parameters which were used to develop the all-elastic behavior curves in Figure 5. The results in Figure 6 show that for the externally stiffened shell, the reduction in maximum load from that obtained in the purely elastic analysis is 23%, whereas the reduction in load-carrying capability for the internally stiffened shell is 15%. Thus, it might be concluded that the effects of eccentricity for longitudinally stiffened cylinders are seen to decrease with the presence of inelastic behavior. This trend was noted by Jones[26] in his study of stiffened shells which buckle initially in the plastic range; it is attributed to the fact that the effective stress is greater for outside stiffened cylindrical shells at maximum load than for cylinders stiffened on the inside. This leads to a larger effective strain for outside stiffened cylinders and, consequently, a greater reduction in maximum load due to inelastic behavior. It should be emphasized that despite the significant reductions in load-carrying capability due to inelastic behavior, the integrally stiffened cylinders of the present analysis buckle well below the 0.2% offset yield stress of the material (stainless steel (1/2 hard)). Therefore, buckling analyses of the types presented in references 5, 6, and 26 are not valid for application to the present maximum-strength problem where, in the absence of initial imperfections, elastic buckling would occur.

After using the stress-strain curve for 2024-T3 aluminum (see Figure 4), it was determined that the reductions in maximum loads of both outside and inside integrally stiffened cylindrical shells (with the geometry shown in Figure 5) from those obtained in the purely elastic analysis were negligible; that is, essentially elastic behavior governed the particular shell analyzed. However, extreme caution should be exercised in any design procedure involving stiffened shell construction wherein plastic buckling is precluded, since large reductions in maximum load can occur for imperfect shells and a variety of materials characterized

by a small exponent (say, 3-5) in the Ramberg-Osgood[20] stress-strain curve representation. This behavior is demonstrated not only in reference 4 but also by the previous results obtained herein for stainless steel cylinders. In addition, for larger values of n and reduced $(R/\bar{t})$ ratios (for example, 75-100), even aluminum cylinders ($N \sim 9$) will bend due to imperfections and reach a maximum strength and fail rather than buckle plastically from the undeformed state.

Correlation between experimental and theoretical results has been achieved by comparing the maximum compressive load of an outside, integrally stiffened, 2024-T3 aluminum cylindrical shell of reference 12 ($L/R = 4$) with the maximum load obtained through the present analysis. Since the stiffened cylinder edges of reference 12 are clamped and those of the present analysis are "effectively" simply supported, the difference between the classical buckling loads for clamped and simply supported edges has been added to the maximum load of the present elastic analysis for an outside, integrally stiffened cylindrical shell. As a result, the maximum load agrees with the experimental maximum load of reference 12 to within 2%.

Therefore, it is believed that sufficient evidence has been given to conclude that, in addition to boundary conditions, initial imperfections, prebuckling deformations, and eccentricity effects, inelastic deformations should not be excluded from initial buckling (maximum strength) analyses of stiffened, circular cylindrical shells in axial compression. In scale structures, the most efficient eccentrically stiffened shell (at least for axial compression) would be one whose $(R/\bar{t})$ ratio precludes plastic buckling, but is not so large for a given material that imperfection sensitivity and inelastic deformation significantly reduce the initial buckling (maximum load). A great deal of experimental work is required on practically fabricated metal shells of various materials in the range $50 < R/t < 250$ to discern the relative effects of stress-strain curve shape and initial imperfections.

CONCLUDING REMARKS

The maximum-strength analysis of initially imperfect, axially compressed, sandwich and eccentrically stiffened, circular cylindrical shells has been undertaken to establish the effects of transverse shear (sandwich case only), inelastic deformations, and geometry dependence on the load-shortening curves for given materials. Although numerical results are given only for the special cases of isotropic sandwich and longitudinally stiffened shells, the theory and solution procedure are applicable to orthotropic shells in general.

CIRCULAR CYLINDRICAL SANDWICH SHELLS

In the absence of inelastic behavior, it is demonstrated that transverse shear deformations reduce the maximum load-carrying capability of an imperfect, isotropic sandwich shell. When inelastic deformations are taken into account, not only is the maximum load further reduced, but the load-shortening curves reflect a significant (R/h)-dependence. This dependence is not evident in any elastic analysis. Future work should be directed toward establishing the effects of inelastic deformations in the core in conjuction with failure not only in general instability (the present analysis) but also in the face-wrinkling modes.

ECCENTRICALLY STIFFENED, CIRCULAR CYLINDRICAL SHELLS

In the absence of inelastic behavior, it is shown that outside stiffened cylindrical shells are capable of carrying higher compressive loads than internally stiffened shells. This result is consistent with those surveyed in references 1-3. However, in the presence of inelastic deformations, the present analysis shows that the load-carrying capability of both outside and inside stiffened, stainless steel (1/2 hard) shells of $R/\bar{t} = 167$ is significantly reduced. Corresponding calculations for 2024-T3 aluminum shells of the same geometry reveal negligible reduction in the maximum load based on purely elastic behavior. Thus, caution should be exercised when dealing with maximum-strength analyses of shells having relatively low exponents (for example, stainless steel, N=3)

in the Ramberg-Osgood stress-strain curve formulation. For shells of materials possessing higher exponents (for example, 2024-T3 aluminum, N = 9), caution should be exercised as the $(R/\bar{t})$ ratio approaches 100. For such shells, initial-imperfection effects are minimized, but plasticity effects are maximized. Until sufficient experimental evidence is developed to prove otherwise, it is believed that the most efficient longitudinally stiffened shells for axial compression loading are those which lie between the plastic buckling failure mode and catastropic snap through failure in a purely elastic mode. In addition, it is shown, on the basis of the stainless steel (1/2 hard) results, that the marked difference between the maximum strengths of outside and inside stiffened cylinders based on all-elastic behavior is significantly reduced when inelastic effects are taken into account. As a result, the choice of outside stiffening to achieve greatly increased elastic-analysis-predicted maximum strength relative to the choice of inside stiffening should be viewed with discretion.

Although limited numerical data are presented herein, the overall results are consistent with those established in reference 4 for unstiffened cylinders in axial compression. That is, regardless of the type of structure (pure monocoque, sandwich, or eccentrically stiffened), it is obvious that any initial buckling (maximum strength) analysis of practically fabricated cylindrical shells must include the effects of initial imperfections, boundary conditions, prebuckling deformations, and inelastic deformations. The material-geometry combination that is the most efficient may be predicted from application of the present theory and analysis procedure for sandwich and eccentrically stiffened shells to a wide variation in physical parameters. However, without substantial experimental effort to establish confidence in the analytical approach, significant weight reduction in aerospace vehicle designs, a major portion of which involve shell structures, will not be realized.

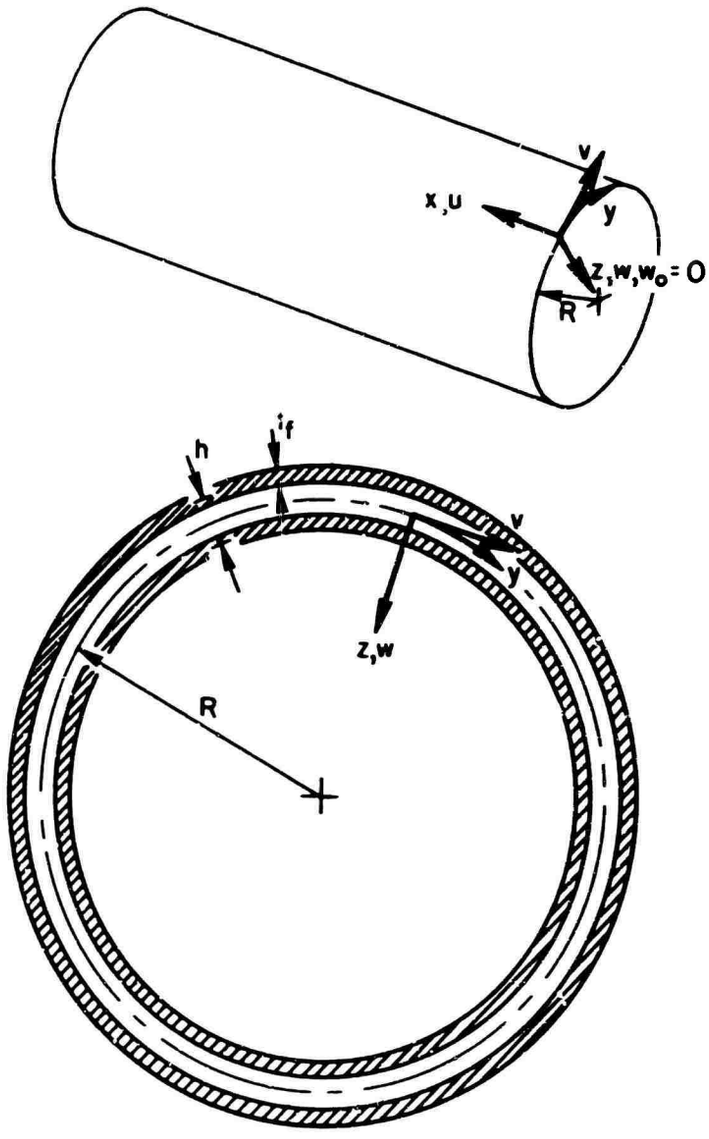

Figure 1. Circular Cylindrical Shell With Two-Element Cross Section.

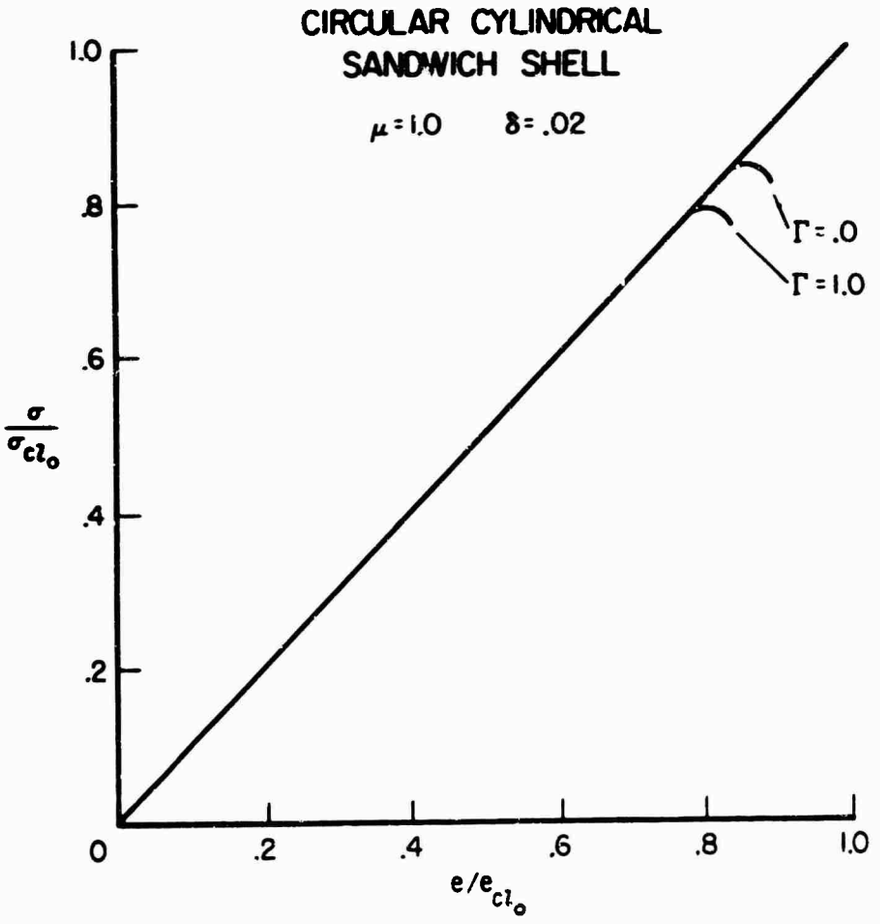

Figure 2. Purely Elastic, Load-Shortening Curves for Isotropic Sandwich, Circular Cylindrical Shells.

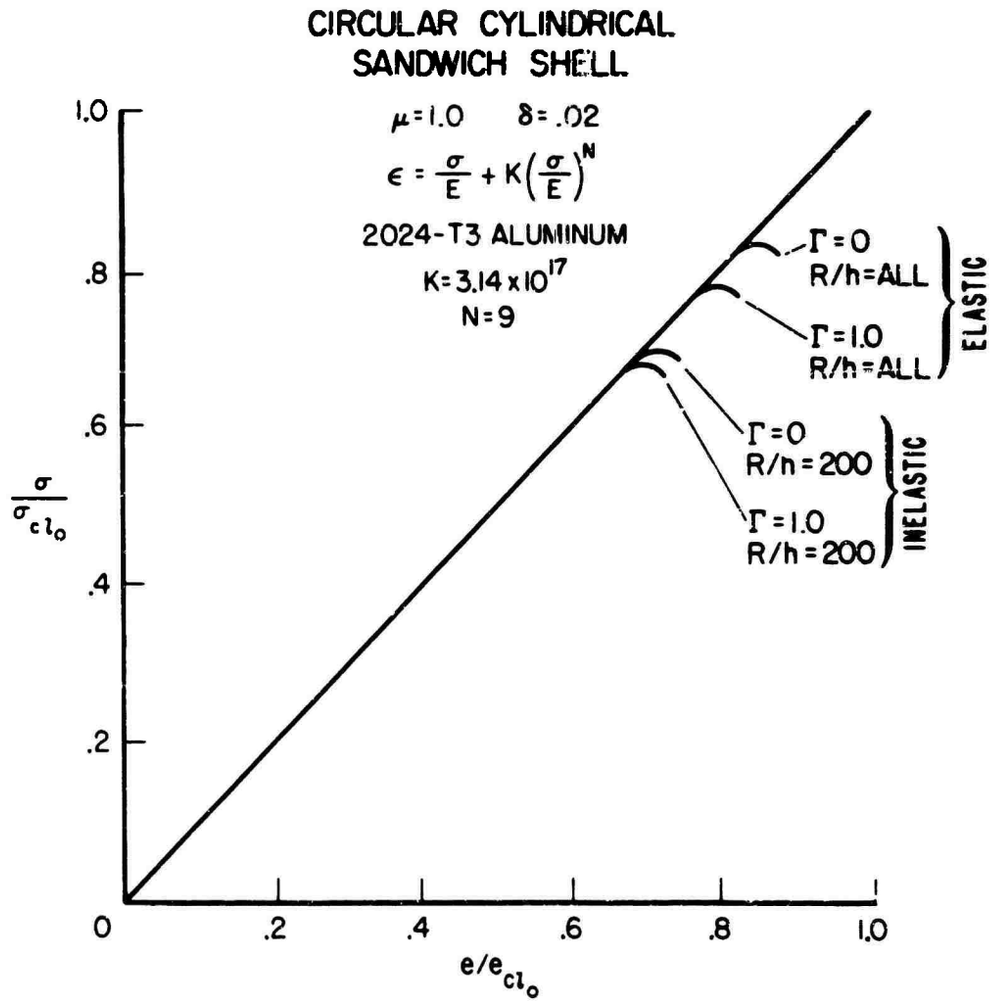

Figure 3. Load-Shortening Curves for 2024-T3 Aluminum, Isotropic Sandwich, Circular Cylindrical Shells.

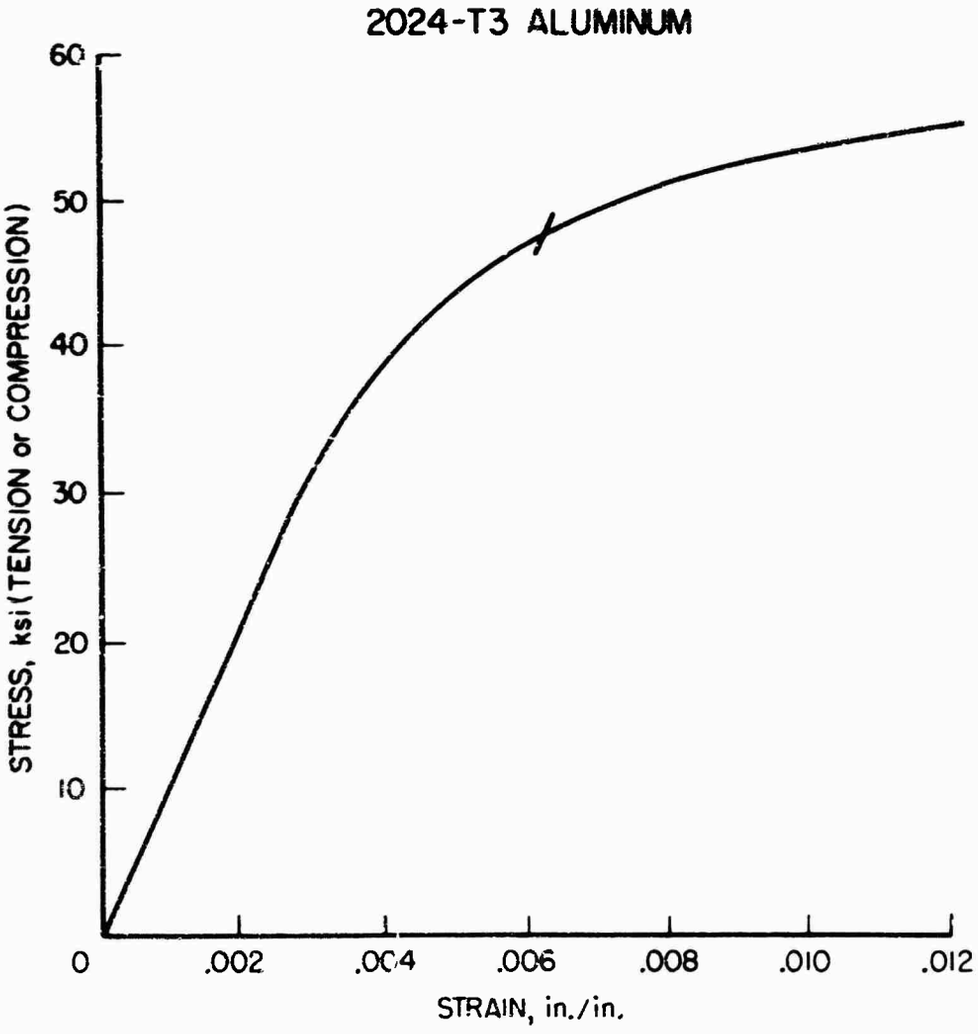

Figure 4. Stress-Strain Curve for 2024-T3 Aluminum.

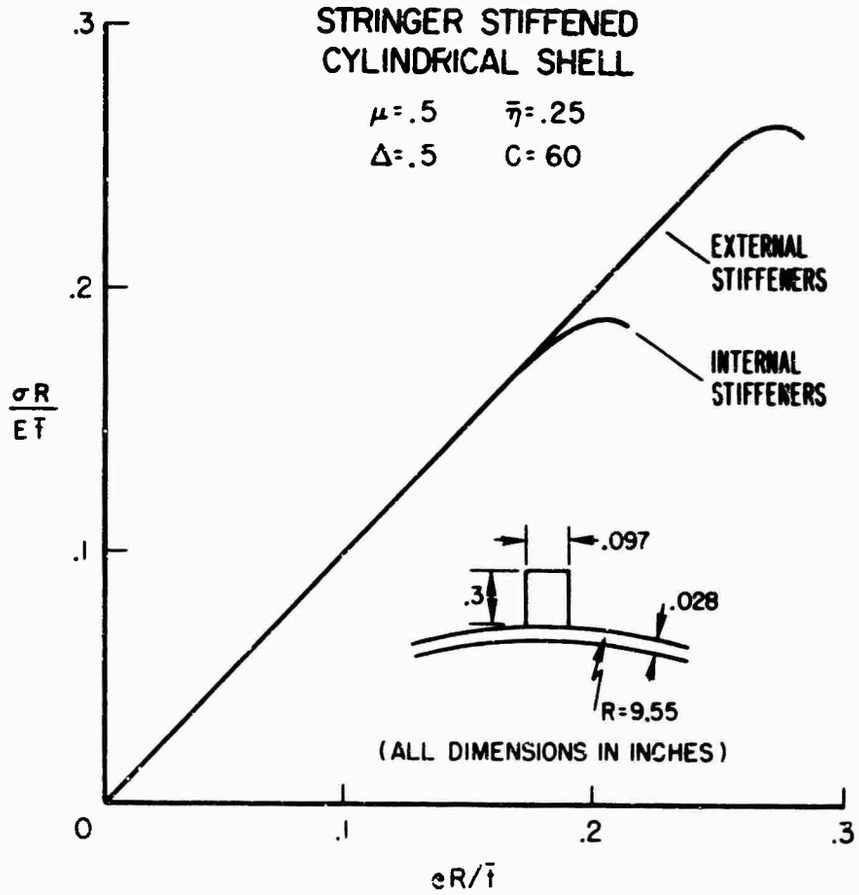

Figure 5. Purely Elastic, Load-Shortening Curves for Eccentrically Stiffened, Circular Cylindrical Shells With Longitudinal Integral Stringers.

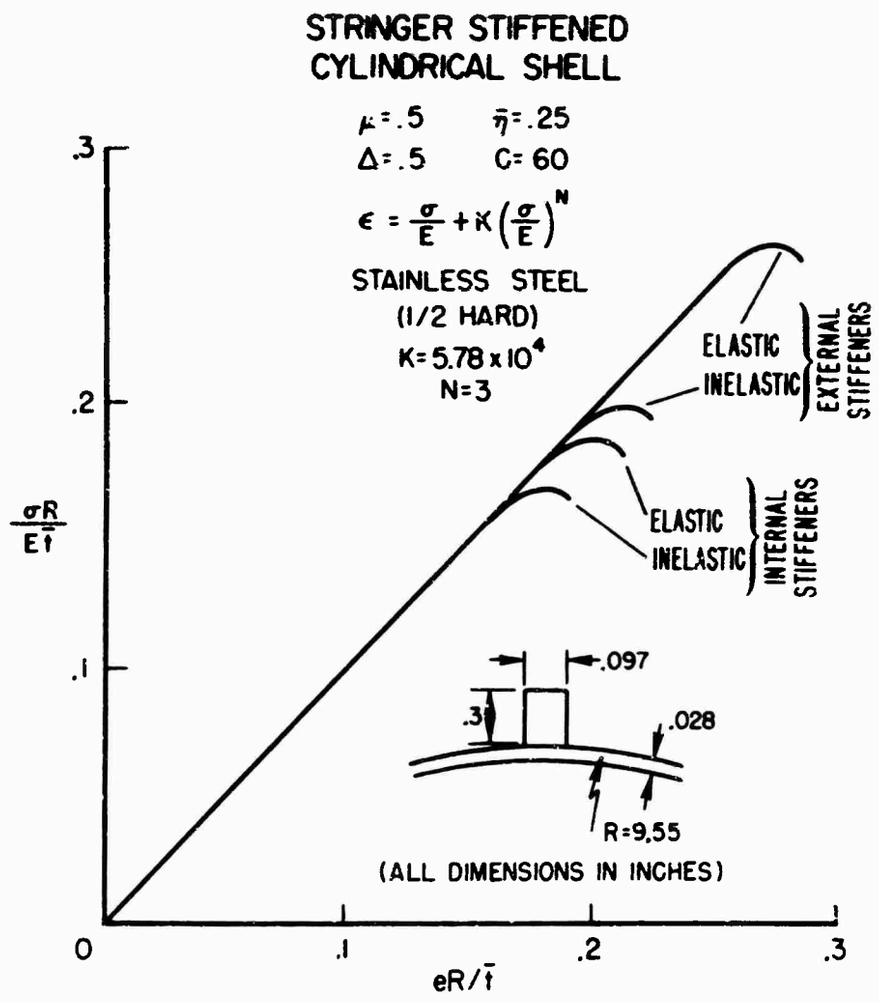

Figure 6. Load-Shortening Curves for Stainless Steel (1/2 Hard), Eccentrically Stiffened, Circular Cylindrical Shells With Longitudinal Integral Stringers.

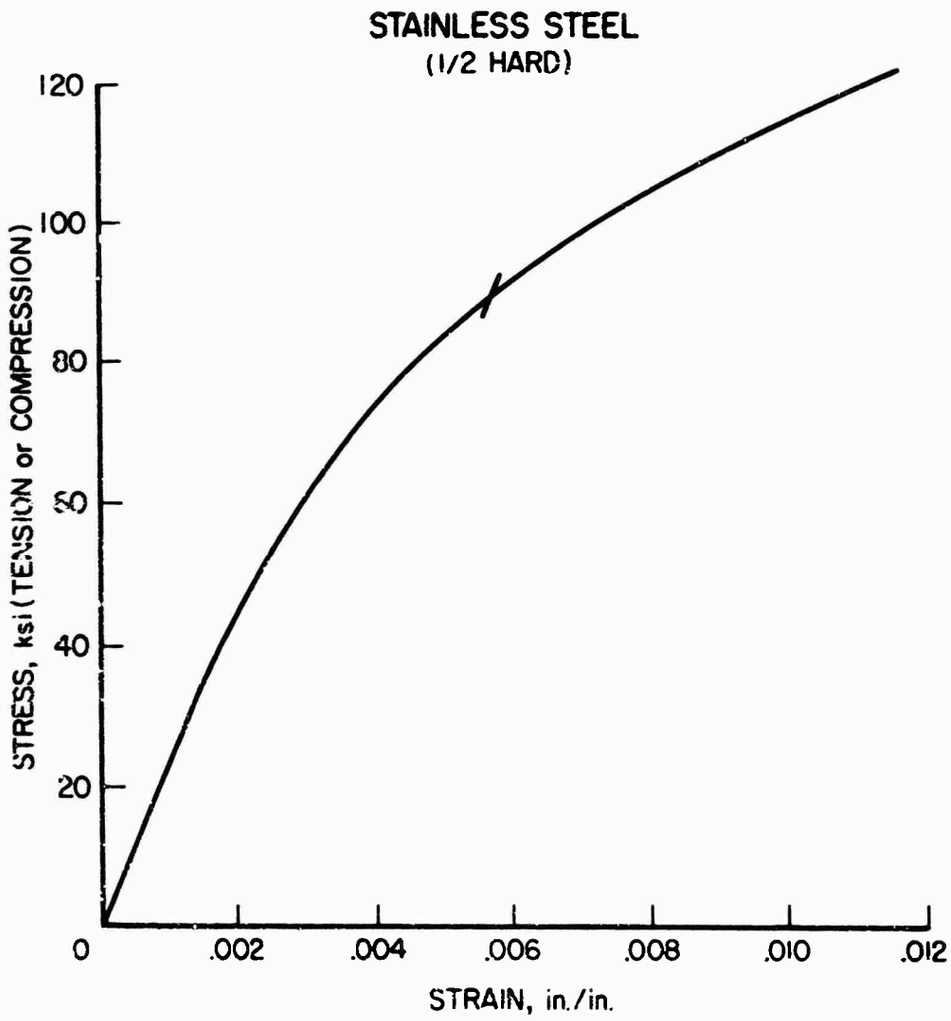

Figure 7. Stress-Strain Curve for Stainless Stell (1/2 Hard).

LITERATURE CITED

1. Hoff, N. J., THIN SHELLS IN AEROSPACE STRUCTURES, Fourth Theodore von Kármán Lecture Presented at the Third AIAA Annual Meeting, Nov. 29, 1966; Aeronautics and Astronautics, Feb. 1967, pp. 26-45.

2. Hoff, N. J., THE PERPLEXING BEHAVIOR OF THIN CIRCULAR CYLINDRICAL SHELLS IN AXIAL COMPRESSION, Second Theodore von Kármán Memorial Lecture of the Israel Society of Aeronautical Sciences, 1966.

3. Stein, M., RECENT ADVANCES IN THE INVESTIGATION OF SHELL BUCKLING, AIAA Journal, Vol. 6, No. 12, December 1968, pp. 2339-2345.

4. Mayers, J. and Wesenberg, D. L., THE MAXIMUM STRENGTH OF INITIALLY IMPERFECT AXIALLY COMPRESSED CIRCULAR CYLINDRICAL SHELLS, Stanford University; USAAVLABS Technical Report 69-60, U.S. Army Aviation Materiel Laboratories, Fort Eustis, Virginia (in publication); (also, presented at the AIAA 7th Aerospace Sciences Meeting, AIAA Paper No. 69-91, New York, January 20-22, 1969).

5. Lee, L. H. N., INELASTIC BUCKLING OF INITIALLY IMPERFECT CYLINDRICAL SHELLS SUBJECT TO AXIAL COMPRESSION, Journal of Aerospace Sciences, January 1962, pp. 87-95.

6. Batterman, S. C., PLASTIC BUCKLING OF AXIALLY COMPRESSED CYLINDRICAL SHELLS, AIAA Journal, Vol. 3, No. 2, February 1965, pp. 316-325.

7. Timoshenko, S., EINIGE STABILITÄTSPROBLEME DER ELASTIZITÄTSTHEORIE, Zeitschrift für Mathematik und Physik, Vol. 58, 1910.

8. Lorenz, R., ACHSENSYMMETRISCHE VERZERRUNGEN IN DÜNNWANDIGEN HOHLZYLINDERN, Zeitschrift des Vereines Deutscher Ingenieure, Vol. 52, 1908.

9. Southwell, R. V., ON THE GENERAL THEORY OF ELASTIC STABILITY, Philosophical Transactions of the Royal Society of London, Series A, Vol. 213, 1914.

10. Peterson, J. P., and Anderson, J. K., STRUCTURAL BEHAVIOR AND BUCKLING STRENGTH OF HONEYCOMB SANDWICH CYLINDERS SUBJECT TO

BENDING, National Aeronautics and Space Administration, NASA Technical Note D-2926, August 1965.

11. Cunningham, J. H., and Jacobson, M. J., DESIGN AND TESTING OF HONEYCOMB SANDWICH CYLINDERS UNDER AXIAL COMPRESSION, Collected Papers on Instability of Shell Structures - 1962, National Aeronautics and Space Administration, NASA Technical Note D-1510, December 1962, pp. 341-359.

12. Card, M. F., and Jones, R. M., EXPERIMENTAL AND THEORETICAL RESULTS FOR BUCKLING OF ECCENTRICALLY STIFFENED CYLINDERS, National Aeronautics and Space Administration, NASA Technical Note D-3639, October 1966.

13. Reissner, E., ON A VARIATIONAL THEOREM IN ELASTICITY, Journal of Mathematics and Physics, Vol. 24, No. 2, July 1950, pp. 90-95.

14. Kempner, J., POSTBUCKLING BEHAVIOR OF AXIALLY COMPRESSED CIRCULAR CYLINDRICAL SHELLS, Journal of Aeronautical Sciences, Vol. 17, May 1954, pp. 329-335, 342.

15. Mayers, J., and Nelson, E., MAXIMUM STRENGTH ANALYSIS OF POSTBUCKLED RECTANGULAR PLATES, Presented at AIAA Sixth Aerospace Sciences Meeting, AIAA Paper No. 68-171, New York, January 1968.

16. Mayers, J., and Rehfield, L. W., Developments in Mechanics, Vol. 3. Part 1, (Proceedings of the Ninth Midwestern Mechanics Conference, Madison, Wisconsin, August 16-18, 1965), John Wiley and Sons, Inc., New York, 1967, pp. 145-160.

17. Mayers, J., and Chu, Y. Y., MAXIMUM LOAD PREDICTION FOR SANDWICH PLATES, Stanford University; USAAVLABS Technical Report 69-3, U.S. Army Aviation Materiel Laboratories, Fort Eustis, Virginia, April 1969, AD 690215.

18. Mayers, J., and Budiansky, B., ANALYSIS OF BEHAVIOR OF SIMPLY SUPPORTED FLAT PLATES COMPRESSED BEYOND BUCKLING INTO THE PLASTIC RANGE, National Advisory Committee for Aeronautics, NACA Technical Note No. 3368, 1955.

19. Mayers, J., Nelson, E., and Smith, L. B., MAXIMUM STRENGTH ANALYSIS OF POSTBUCKLED RECTANGULAR PLATES, Stanford University, Department of Aeronautics and Astronautics Report, SUDAAR No. 215, December 1964.

20. Ramberg, W., and Osgood, W. R., DESCRIPTION OF STRESS-STRAIN CURVES BY THREE PARAMETERS, National Advisory Committee for Aeronautics, NACA Technical Note No. 902, 1943.

21. Mayers, J., and Wrenn, B. G., DEVELOPMENTS IN MECHANICS, Vol. 4, (Proceedings of the Tenth Midwestern Mechanics Conference, Fort Collins, Colorado, August 21-23, 1967), Johnson Publishing Co., 1968, pp. 819-846.

22. Tennyson, R. C., and Welles, S. W., ANALYSIS OF THE BUCKLING PROCESS OF CIRCULAR CYLINDRICAL SHELLS UNDER AXIAL COMPRESSION, Institute of Aerospace Studies, University of Toronto, February 1968. (In process of publication in AIAA Journal).

23. Block, D. L., Card, M. F., and Mikulas, M. M., BUCKLING OF ECCENTRICALLY STIFFENED ORTHOTROPIC CYLINDERS, National Aeronautics and Space Administration, NASA Technical Note D-2960, August 1965.

24. Stein, M., and Mayers, J., COMPRESSIVE BUCKLING OF SIMPLY SUPPORTED CURVED PLATES AND CYLINDERS OF SANDWICH CONSTRUCTION, National Advisory Committee for Aeronautics, NACA Technical Note No. 2601, January 1952.

25. Hutchinson, J. W., and Amazigo, J. C., IMPERFECTION-SENSITIVITY OF ECCENTRICALLY STIFFENED CYLINDRICAL SHELLS, AIAA Journal, Vol. 5, No. 3, March 1967, pp. 392-401.

26. Jones, R. M., PLASTIC BUCKLING OF ECCENTRICALLY STIFFENED CIRCULAR CYLINDRICAL SHELLS, AIAA Journal, Vol. 5, No. 6, June 1967, pp. 1147-1152.

27. Yoshimura, Y., ON THE MECHANISM OF BUCKLING OF A CIRCULAR CYLINDRICAL SHELL UNDER AXIAL COMPRESSION, National Advisory Committee for Aeronautics, NACA Technical Memorandum No. 1390, Washington, D. C., July 1955.

APPENDIX I

EULER EQUATIONS AND BOUNDARY CONDITIONS DERIVED FROM A REISSNER FUNCTIONAL FOR A SANDWICH CYLINDER WITH PRESCRIBED END SHORTENING

The Reissner functional for prescribed end shortening is defined as

$$U'' = \iiint_V (\sigma_x \epsilon_x + \sigma_y \epsilon_y + \tau_{xy}\gamma_{xy} + \tau_{xz}\gamma_{xz} + \tau_{yz}\gamma_{yz} - F')\, dV \tag{44}$$

The von Kármán-Donnell strain-displacement relations, modified for the two-element cylinder (see Figure 1), and including initial radial deformation and transverse shear effects, are

$$\epsilon_{x_{t,b}} = \epsilon'_x \pm \epsilon''_x = u_{,x} + \frac{1}{2} w_{,x}^2 + w_{o,x} w_{,x} \pm \frac{h}{2} (w_{,xx} - \gamma_{xz,x})$$

$$\epsilon_{y_{t,b}} = \epsilon'_y \pm \epsilon''_y = v_{,y} + \frac{1}{2} w_{,y}^2 + w_{o,y} w_{,y} - \frac{w}{R} \pm \frac{h}{2} (w_{,yy} - \gamma_{yz,y})$$

$$\gamma_{xy_{t,b}} = \gamma'_{xy} \pm \gamma''_{xy} = u_{,y} + v_{,x} + w_{,x} w_{,y} + w_{o,x} w_{,y} + w_{o,y} w_{,x}$$

$$\pm h(w_{,xy} - \frac{1}{2} \gamma_{xz,y} - \frac{1}{2} \gamma_{yz,x}) \tag{45}$$

The stresses in the top and bottom faces in terms of the midsurface and bending components are

$$\sigma_{x_{t,b}} = \sigma'_x \pm \sigma''_x$$

$$\sigma_{y_{t,b}} = \sigma'_y \pm \sigma''_y \tag{46}$$

$$\tau_{xy_{t,b}} = \tau'_{xy} \pm \tau''_{xy}$$

After integration through the top and bottom faces and the core of the sandwich cross section, equation (44) becomes

$$U'' = t_f \int_0^L \int_0^{2\pi R} \left\{ \sigma_{x_t} \epsilon_{x_t} + \sigma_{x_b} \epsilon_{x_b} + \sigma_{y_t} \epsilon_{y_t} + \sigma_{y_b} \epsilon_{y_b} \right.$$

$$+ \tau_{xy_t}\gamma_{xy_t} + \tau_{xy_b}\gamma_{xy_b} + \frac{t_c}{t_f}\left(\tau_{xz}\gamma_{xz} + \tau_{yz}\gamma_{yz}\right) - \left(F'_t + F'_b\right)$$

$$- \frac{t_c}{t_f} F'_c \Bigg\} \, dxdy \tag{47}$$

Substitution of equation (45) into equation (47) leads to

$$U'' = t_f \int_0^L \int_0^{2\pi R} \Bigg\{ \left(\sigma_{x_t} + \sigma_{x_b}\right) \left[u_{,x} + \frac{1}{2} w_{,x}^2 + w_{,x} w_{o,x} \right]$$

$$+ \left(\sigma_{y_t} + \sigma_{y_b}\right) \left[v_{,y} + \frac{1}{2} w_{,y}^2 + w_{,y} w_{o,y} - \frac{w}{R} \right]$$

$$+ \left(\tau_{xy_t} + \tau_{xy_b}\right) \left[v_{,x} + u_{,y} + w_{,x} w_{,y} + w_{,x} w_{o,y} + w_{,y} w_{o,x} \right]$$

$$+ \left(\sigma_{x_t} - \sigma_{x_b}\right)\frac{h}{2} \left[w_{,xx} - \gamma_{xz,x} \right] + \left(\sigma_{y_t} - \sigma_{y_b}\right)\frac{h}{2} \left[w_{,yy} - \gamma_{yz,y} \right]$$

$$+ \left(\tau_{xy_t} - \tau_{xy_b}\right) h \left[w_{,xy} - \frac{1}{2}\gamma_{xz,y} - \frac{1}{2}\gamma_{yz,x} \right] + \frac{t_c}{t_f} \left[\tau_{xz}\gamma_{xz}$$

$$+ \tau_{yz}\gamma_{yz} \right] - \frac{1}{2}\frac{t_c}{t_f} \left[\frac{\tau_{xz}^2}{G_{xz}} + \frac{\tau_{yz}^2}{G_{yz}} \right] - \left(F'_t + F'_b\right) \Bigg\} \, dxdy \tag{48}$$

The average stresses and the bending moments are

$$\sigma'_x = \frac{1}{2}\left(\sigma_{x_t} + \sigma_{x_b}\right)$$

$$\sigma'_y = \frac{1}{2}\left(\sigma_{y_t} + \sigma_{y_b}\right)$$

$$\tau'_{xy} = \frac{1}{2}\left(\tau_{xy_t} + \tau_{xy_b}\right) \tag{49}$$

$$M_x = -t_f \frac{h}{2}\left(\sigma_{x_t} - \sigma_{x_b}\right) = -t_f h \sigma''_x$$

$$M_y = -t_f \frac{h}{2}\left(\sigma_{y_t} - \sigma_{y_b}\right) = -t_f h \sigma''_y$$

$$M_{xy} = t_f \frac{h}{2} (\tau_{xy_t} - \tau_{xy_b}) = t_f h \tau''_{xy} \tag{49}$$

Substitution of equation (49) into equation (48) gives

$$\begin{aligned} U'' = 2t_f \int_0^L \int_0^{2\pi R} \Big\{ & \sigma'_x (u_{,x} + \tfrac{1}{2} w_{,x}^2 + w_{,x} w_{o,x}) \\ & + \sigma'_y (v_{,y} + \tfrac{1}{2} w_{,y}^2 + w_{,y} w_{o,y} - \tfrac{w}{R}) + \tau'_{xy} (u_{,y} + v_{,x} + w_{,x} w_{,y} \\ & + w_{o,x} w_{,y} + w_{o,y} w_{,x}) - \frac{M_x}{2t_f} (w_{,xx} - \gamma_{xz,x}) - \frac{M_y}{2t_f} (w_{,yy} - \gamma_{yz,y}) \\ & + \frac{M_{xy}}{t_f} (w_{,xy} - \tfrac{1}{2} \gamma_{xz,y} - \tfrac{1}{2} \gamma_{yz,x}) + \frac{t_c}{2t_f} (\tau_{xz}\gamma_{xz} + \tau_{yz}\gamma_{yz}) \\ & - \frac{1}{4} \frac{t_c}{t_f} \left(\frac{\tau_{xz}^2}{G_{xz}} + \frac{\tau_{yz}^2}{G_{yz}} \right) - F' \Big\} \, dx dy \end{aligned} \tag{50}$$

with cognizance taken of the fact that

$$\delta F = \frac{\partial F'}{\partial \sigma'_x} \delta\sigma'_x + \frac{\partial F'}{\partial \sigma'_y} \delta\sigma'_y + \frac{\partial F'}{\partial \tau'_{xy}} \delta\tau'_{xy} + \frac{\partial F'}{\partial M_x} \delta M_x + \frac{\partial F'}{\partial M_y} \delta M_y + \frac{\partial F'}{\partial M_{xy}} \delta M_{xy}$$

The vanishing of the first variation of U'' with respect to σ'_x, σ'_y, τ'_{xy}, τ_{xz}, τ_{yz}, M_x, M_y, M_{xy}, u, v, w, γ_{xz}, and γ_{yz} requires that

$$\begin{aligned} \delta U'' = 2t_f \int_0^L \int_0^{2\pi R} \Big\{ & \delta\sigma_x (u_{,x} + \tfrac{1}{2} w_{,x}^2 + w_{,x} w_{o,x}) + \delta\sigma_y (v_{,y} \\ & + \tfrac{1}{2} w_{,y}^2 + w_{,y} w_{o,y} - \tfrac{w}{R}) + \delta\tau'_{xy} (u_{,y} + v_{,x} + w_{,x} w_{,y} \\ & + w_{o,x} w_{,y} + w_{o,y} w_{,x}) + \sigma_x (\delta u_{,x} + w_{,x} \delta w_{,x} + \delta w_{,x} w_{o,x}) \\ & + \sigma_y (\delta v_{,y} + w_{,y} \delta w_{,y} + \delta w_{,y} w_{o,y} - \tfrac{\delta w}{R}) + \tau_{xy} (\delta u_{,y} + \delta v_{,x} \\ & + \delta w_{,x} w_{,y} + \delta w_{,y} w_{,x} + \delta w_{,x} w_{o,y} + \delta w_{,y} w_{o,x}) - \frac{\delta M_x}{2t_f} (w_{,xx} \\ & - \gamma_{xz,x}) - \frac{\delta M_y}{2t_f} (w_{,yy} - \gamma_{yz,y}) - \frac{\delta M_{xy}}{f} (w_{,xy} \end{aligned} \tag{51}$$

$$- \frac{1}{2}\gamma_{xz,y} - \frac{1}{2}\gamma_{yz,x}) - \frac{M_x}{2t_f}(\delta w_{,xx} - \delta\gamma_{xz,x}) - \frac{M_y}{2t_f}(\delta w_{,yy}$$

$$- \delta\gamma_{yz,y}) + \frac{M_{xy}}{t_f}(\delta w_{,xy} - \frac{1}{2}\delta\gamma_{xz,y} - \frac{1}{2}\delta\gamma_{yz,x}) + \frac{t_c}{2t_f}(\delta\tau_{xz}\gamma_{xz}$$

$$+ \delta\tau_{yz}\gamma_{yz} + \tau_{xz}\delta\gamma_{xz} + \tau_{yz}\delta\gamma_{yz}) - \frac{1}{2}\frac{t_c}{t_f}\left(\frac{\tau_{xz}}{G_{xz}}\delta\tau_{xz} + \frac{\tau_{yz}}{G_{yz}}\delta\tau_{yz}\right) - \frac{\partial F'}{\partial\sigma'_x}\delta\sigma'_x$$

$$- \frac{\partial F'}{\partial\sigma'_y}\delta\sigma'_y - \frac{\partial F'}{\partial\tau'_{xy}}\delta\tau'_{xy} - \frac{\partial F'}{\partial M_x}\delta M_x - \frac{\partial F'}{\partial M_y}\delta M_y - \frac{\partial F'}{\partial M_{xy}}\delta M_{xy}\Bigg\} dxdy = 0 \tag{51}$$

Integration by parts, as appropriate, leads to

$$\delta U'' = 2t_f \int_0^L \int_0^{2\pi R} \Bigg\{\left(u_{,x} + \frac{1}{2}w_{,x}^2 + w_{,x}w_{o,x} - \frac{\partial F'}{\partial\sigma'_x}\right)\delta\sigma'_x$$

$$+ \left(v_{,y} + \frac{1}{2}w_{,y}^2 + w_{,y}w_{o,y} - \frac{w}{R} - \frac{\partial F'}{\partial\sigma'_y}\right)\delta\sigma'_y + \left(u_{,y} + v_{,x}\right.$$

$$\left. + w_{,x}w_{,y} + w_{o,x}w_{,y} + w_{o,y}w_{,x} - \frac{\partial F'}{\partial\tau'_{xy}}\right)\delta\tau'_{xy} - \left[\frac{1}{2t_f}\left(w_{,xx}\right.\right.$$

$$\left.\left. - \gamma_{xz,x}\right) + \frac{\partial F'}{\partial M_x}\right]\delta M_x - \left[\frac{1}{2t_f}\left(w_{,yy} - \gamma_{yz,y}\right) + \frac{\partial F'}{\partial M_y}\right]\delta M_y$$

$$+ \left[\frac{1}{t_f}\left(w_{,xy} - \frac{1}{2}\gamma_{xz,y} - \frac{1}{2}\gamma_{yz,x}\right) - \frac{\partial F'}{\partial M_{xy}}\right]\delta M_{xy}$$

$$- \left(\sigma'_{x,x} + \tau'_{xy,y}\right)\delta u - \left(\sigma'_{y,y} + \tau'_{xy,x}\right)\delta v - \left[\left(\sigma'_x\left[w_{,x}\right.\right.\right.$$

$$\left.\left.\left. + w_{o,x}\right]\right)_{,x} + \left(\sigma'_y\left[w_{,y} + w_{o,y}\right]\right)_{,y}\right.$$

$$+ \left(\tau'_{xy}\left[w_{,y} + w_{o,y}\right]\right)_{,x} + \left(\tau'_{xy}\left[w_{,x} + w_{o,x}\right]\right)_{,y}$$

$$\left. - \frac{\sigma'_y}{R} + \frac{1}{2t_f}\left(M_{x,xx} + M_{y,yy} - 2M_{xy,xy}\right)\right]\delta w - \frac{1}{2t_f}\left[M_{x,x}\right.$$

$$- M_{xy,y} - t_c \tau_{xz} \Big] \delta\gamma_{xz} - \frac{1}{2t_f} \Big[M_{y,y} - M_{xy,x} - t_c \tau \Big] \delta\gamma_{yz}$$

$$+ \frac{t_c}{2t_f} \left[\gamma_{xz} - \frac{\tau_{xz}}{G_{xz}} \right] \delta \tau_{xz} + \frac{t_c}{2t_f} \left[\gamma_{yz} - \frac{\tau_{yz}}{G_{yz}} \right] \delta \tau_{yz} \Bigg\} dxdy$$

$$+ 2t_f \int_0^{2\pi R} \sigma'_x \, \delta u \Big|_0^L dy + 2t_f \int_0^L \sigma'_y \, \delta v \Big|_0^{2\pi R} dx$$

$$+ 2t_f \int_0^{2\pi R} \Big[\sigma'_x \left(w_{,x} + w_{o,x} \right) + \tau'_{xy} \left(w_{,y} + w_{o,y} \right) + \frac{1}{2t_f} M_{x,x}$$

$$- \frac{1}{t_f} M_{xy,y} \Big] \delta w \Big|_0^L dy + 2t_f \int_0^L \Big[\sigma'_y \left(w_{,y} + w_{o,y} \right)$$

$$+ \tau'_{xy} \left(w_{,x} + w_{o,x} \right) + \frac{1}{2t_f} M_{y,y} - \frac{1}{t_f} M_{xy,x} \Big] \delta w \Big|_0^{2\pi R} dx$$

$$+ 2t_f \int_0^{2\pi R} \tau'_{xy} \, \delta v \Big|_0^L dy + 2t_f \int_0^L \tau'_{xy} \, \delta u \Big|_0^{2\pi R} dx - \int_0^{2\pi R} M_x \, \delta w_{,x} \Big|_0^L dy$$

$$- \int_0^L M_y \, \delta w_{,y} \Big|_0^{2\pi R} dx + 2M_{xy} \, \delta w \Big|_0^L \Big|_0^{2\pi R} + \int_0^{2\pi R} M_x \, \delta\gamma_{xz} \Big|_0^L dy$$

$$+ \int_0^L M_y \, \delta\gamma_{yz} \Big|_0^{2\pi R} dx - \int_0^L M_{xy} \, \delta\gamma_{xz} \Big|_0^{2\pi R} dx - \int_0^{2\pi R} M_{xy} \, \delta\gamma_{yz} \Big|_0^L dy = 0 \tag{52}$$

For equation (52) to vanish for simultaneous arbitrary variations in the states of stress and displacement, each of the above terms must

vanish independently. The resulting Euler equations and stress-displacement relations are

$$\frac{\partial F'}{\partial \varepsilon'_x} = u_{,x} + \frac{1}{2} w_{,x}^2 + w_{o,x} w_{,x}$$

$$\frac{\partial F'}{\partial \varepsilon'_y} = v_{,y} + \frac{1}{2} w_{,y}^2 + w_{o,y} w_{,y} - \frac{w}{R} \qquad (53)$$

$$\frac{\partial F'}{\partial \varepsilon'_{xy}} = u_{,y} + v_{,x} + w_{,x} w_{,y} + w_{o,x} w_{,y} + w_{,x} w_{o,y}$$

Moment-curvature relations with transverse shear effects are

$$\frac{\partial F'}{\partial M_x} = -\frac{1}{2t_f}\left(\phi_{x,x} - \gamma_{xz,x}\right)$$

$$\frac{\partial F'}{\partial M_y} = -\frac{1}{2t_f}\left(\phi_{y,y} - \gamma_{yz,y}\right) \qquad (54)$$

$$\frac{\partial F'}{\partial M_{xy}} = \frac{1}{t_f}\left(\phi_{x,y} - \frac{1}{2}\gamma_{xz,y} - \frac{1}{2}\gamma_{yz,x}\right)$$

Midsurface equilibrium equations are

$$\sigma'_{x,x} + \sigma'_{xy,y} = 0$$

$$\sigma'_{xy,x} + \sigma'_{y,y} = 0 \qquad (55)$$

Core-shear equilibrium equations are

$$M_{x,x} - M_{xy,y} - t_c \tau_{xz} = 0$$

$$M_{y,y} - M_{xy,x} - t_c \tau_{yz} = 0 \qquad (56)$$

Lateral equilibrium equation is

$$\sigma^{\circ}_{x}\,(w_{,x} + w_{o,x})\,\sigma_{x} - \sigma^{\circ}_{y}\,(w_{,y} + w_{o,y})\,\sigma_{y}$$

$$+ \sigma^{\circ}_{xy}\,(w_{,y} + w_{o,y})\,\sigma_{x} + \sigma^{\circ}_{xy}\,(w_{,x} + w_{o,x})\,\sigma_{y} \qquad (57)$$

$$+ \frac{\sigma^{\circ}}{R} + \frac{1}{2t_{f}}\,(M_{x,xx} + M_{y,yy} - 2M_{xy,xy}) = 0$$

Substitution of equation (55) into equation (57) leads to the simplified, lateral equilibrium equation

$$\sigma^{\circ}_{x}\,(w_{,xx} + w_{o,xx}) + \sigma^{\circ}_{y}\,(w_{,yy} + w_{o,yy}) + 2\sigma^{\circ}_{xy}\,(w_{,xy} + w_{o,xy})$$

$$+ \frac{\sigma^{\circ}}{R} + \frac{1}{2t_{f}}\,(M_{x,xx} + M_{y,yy} - 2M_{xy,xy}) = 0 \qquad (58)$$

Transverse shear stress-strain relations are

$$\sigma_{xz} = G_{xz}\gamma_{xz}$$

$$\sigma_{yz} = G_{yz}\gamma_{yz} \qquad (59)$$

The midsurface stress-displacement boundary integrals are

$$\int_{0}^{2\pi R} \sigma^{\circ}_{x}\,\delta u \Big|_{0}^{L}\,dy \qquad (60a)$$

$$\int_{0}^{L} \sigma^{\circ}_{y}\,\delta w \Big|_{0}^{2\pi R}\,dx \qquad (60b)$$

$$\int_{0}^{2\pi R} \sigma^{\circ}_{xy}\,\delta w \Big|_{0}^{L}\,dy \qquad (60c)$$

$$\int_{0}^{L} \sigma^{\circ}_{xy}\,\delta u \Big|_{0}^{2\pi R}\,dx \qquad (60d)$$

The remaining boundary integrals are

$$\int_0^{2\pi R} \left[\sigma_x^* (w_{,x} + w_{o,x}) + \tau_{xy}^* (w_{,y} + w_{o,y}) + \frac{1}{2t_c} M_{x,x} \right.$$

$$\left. - \frac{1}{t_f} M_{xy,y} \right] \delta w \Big|_0^L dy = 0 \tag{61a}$$

$$\int_0^{L} \left[\sigma_y^* (w_{,y} + w_{o,y}) + \tau_{xy}^* (w_{,x} + w_{o,x}) + \frac{1}{2t_c} M_{y,y} \right.$$

$$\left. - \frac{1}{t_f} M_{xy,x} \right] \delta w \Big|_0^{2\pi R} dx = 0 \tag{61b}$$

$$\int_0^{2\pi R} M_x \, \delta w_{,x} \Big|_0^L dy = 0 \tag{61c}$$

$$\int_0^{L} M_y \, \delta w_{,y} \Big|_0^{2\pi R} dx = 0 \tag{61d}$$

$$M_{xy} \, \delta w \Big|_0^L \Big|_0^{2\pi R} = 0 \tag{61e}$$

$$\int_0^{2\pi R} M_x \, \delta \gamma_{xz} \Big|_0^L dy = 0 \tag{61f}$$

$$\int_0^{L} M_y \, \delta \gamma_{yz} \Big|_0^{2\pi R} dx = 0 \tag{61g}$$

$$\int_0^{L} M_{xy} \, \delta \gamma_{xz} \Big|_0^{2\pi R} dx = 0 \tag{61h}$$

$$\int_0^{2\pi R} M_{xy} \, \delta \gamma_{yz} \Big|_0^L dy = 0 \tag{61i}$$

Since the end shortening is prescribed, δu vanishes at $x = 0, L$. The remaining boundary integrals, evaluated at $x = 0,L$, can be ignored due to the very large L/R ratio assumed for the sandwich cylindrical

shell. The boundary conditions at $y = 0, 2\pi R$ are either continuity conditions or conditions which preclude any resultant shear or circumferential load along any generator after subsequent integration over the shell length.

APPENDIX II

EULER EQUATIONS AND BOUNDARY CONDITIONS DERIVED FROM THE REISSNER FUNCTIONAL FOR AN ORTHOTROPIC, TWO-ELEMENT CYLINDER WITH PRESCRIBED END SHORTENING

The Reissner functional for prescribed end shortening is

$$U'' = \iiint_V (\sigma_x \epsilon_x + \sigma_y \epsilon_y + \tau_{xy} \gamma_{xy} - F^*)\, dV \tag{62}$$

where the core of the two-element cylinder has been assumed rigid in shear.

The von Kármán-Donnell strain displacement relations for the orthotropic, two-element cylinder, modified to include initial radial imperfections, are

$$\epsilon_{x_{t,b}} = \epsilon'_x \pm \epsilon''_x = u_{,x} + \frac{1}{2} w_{,x}^2 + w_{,x} w_{o,x} \pm \frac{h_x}{2} w_{,xx}$$

$$\epsilon_{y_{t,b}} = \epsilon'_y \pm \epsilon''_y = v_{,y} + \frac{1}{2} w_{,y}^2 + w_{,y} w_{o,y} - \frac{w}{R} \pm \frac{h_y}{2} w_{,yy} \tag{63}$$

$$\gamma_{xy_{t,b}} = \gamma'_{xy} \pm \gamma''_{xy} = u_{,y} + v_{,x} + w_{,x} w_{,y} + w_{o,x} w_{,y} + w_{o,y} w_{,x} \pm h_{xy} w_{,xy}$$

where h_x, h_y, and h_{xy} are introduced to account for bending stiffness orthotropy. The distances h_x and h_y separate the faces normal to the x- and y-directions, respectively, and h_{xy} is a fictitious weighted average of h_x and h_y. The orthotropic bending stiffnesses are related to h_x, h_y, and h_{xy} in the following way:

$$D_x = \frac{E t_f h_x^2}{2}$$

$$D_y = \frac{F t_f h_y^2}{2} \tag{64}$$

$$D_{xy} = \frac{E t_f h_{xy}^2}{2\left(1 + \frac{\nu_x}{2} + \frac{\nu_y}{2}\right)} \tag{64}$$

The stiffnesses D_x, D_y, and D_{xy} could be obtained, for example, from laboratory tests on the particular orthotropic structure of interest.

The stresses in terms of midsurface and bending components are

$$\sigma_{x_{t,b}} = \sigma'_x \pm \sigma''_x$$

$$\sigma_{y_{t,b}} = \sigma'_y \pm \sigma''_y \tag{65}$$

$$\tau_{xy_{t,b}} = \tau'_{xy} \pm \tau''_{xy}$$

After integration through the top and bottom faces of the two-element section, equation (62) becomes

$$U'' = t_f \int_0^L \int_0^{2\pi R} \Big| \sigma_{x_t} \epsilon_{x_t} + \sigma_{x_b} \epsilon_{x_b} + \sigma_{y_t} \epsilon_{y_t} + \sigma_{y_b} \epsilon_{y_b} + \tau_{xy_t} \gamma_{xy_t} + \tau_{xy_b} \gamma_{xy_b} - (F'_t + F'_b) \Big| \, dx\,dy \tag{66}$$

Substitution of equation (63) into equation (66) gives

$$\begin{aligned} U'' = t_f \int_0^L \int_0^{2\pi R} \Big| & (\sigma_{x_t} + \sigma_{x_b}) \left[u_{,x} + \frac{1}{2} w_{,x}^2 + w_{,x} w_{o,x}\right] \\ & + (\sigma_{y_t} + \sigma_{y_b}) \left[v_{,y} + \frac{1}{2} w_{,y}^2 + w_{o,y} w_{,y} - \frac{w}{R}\right. \\ & + (\tau_{xy_t} + \tau_{xy_b}) \left[v_{,x} + u_{,y} + w_{,x} w_{,y} + w_{,x} w_{o,y} + w_{o,x} w_{,y}\right] \\ & + (\sigma_{x_t} - \sigma_{x_b}) \frac{h_x}{2} w_{,xx} + (\sigma_{y_t} - \sigma_{y_b}) \frac{h_y}{2} w_{,yy} \end{aligned}$$

$$+ (\tau_{xy_t} - \tau_{xy_b})\, h_{xy} w_{,xy} - (F'_t + F'_b) \Big\} \, dxdy \tag{67}$$

The average stresses and bending moments are

$$\sigma'_x = \frac{1}{2}(\sigma_{x_t} + \sigma_{x_b})$$

$$\sigma'_y = \frac{1}{2}(\sigma_{y_t} + \sigma_{y_b})$$

$$\tau'_{xy} = \frac{1}{2}(\tau_{xy_t} + \tau_{xy_b})$$

$$M_x = -t_f \frac{h_x}{2}(\sigma_{x_t} - \sigma_{y_b}) = -t_f h_x \sigma''_x \tag{68}$$

$$M_y = -t_f \frac{h_y}{2}(\sigma_{y_t} - \sigma_{y_b}) = -t_f h_y \sigma''_y$$

$$M_{xy} = t_f \frac{h_{xy}}{2}(\tau_{xy_t} - \tau_{xy_b}) = t_f h_{xy} \tau''_{xy}$$

Substitution of equation (68) into equation (67) yields

$$U'' = 2t_f \int_0^L \int_0^{2\pi R} \Big\{ \sigma'_x (u_{,x} + \frac{1}{2} w_{,x}^2 + w_{,x} w_{o,x}$$

$$+ \sigma'_y (v_{,y} + \frac{1}{2} w_{,y}^2 + w_{,y} w_{o,y} - \frac{w}{R})$$

$$+ \tau'_{xy} (u_{,y} + v_{,x} + w_{,y} w_{,x} + w_{o,x} w_{,y} + w_{o,y} w_{,x})$$

$$- \frac{M_x}{2t_f} w_{,xx} - \frac{M_y}{2t_f} w_{,yy} + \frac{M_{xy}}{t_f} w_{,xy} - F' \Big\} \, dxdy \tag{69}$$

which is identical to that derived in reference 4.

The vanishing of the first variation of U'' with respect to σ'_x, σ'_y, τ'_{xy}, M_x, M_y, M_{xy}, u, v, and w leads to the Euler equations and

boundary conditions, which are derived in detail in reference 4.

Stress-displacement relations:

$$\frac{\partial F'}{\partial \sigma'_x} = u_{,x} + \frac{1}{2} w_{,x}^2 + w_{,x} w_{o,x}$$

$$\frac{\partial F'}{\partial \sigma'_y} = v_{,y} + \frac{1}{2} w_{,y}^2 + w_{,y} w_{o,y} \tag{70}$$

$$\frac{\partial F'}{\partial \tau'_{xy}} = v_{,x} + u_{,y} + w_{,x} w_{,y} + w_{o,x} w_{,y} + w_{o,y} w_{,x}$$

Moment curvature relations are

$$\frac{\partial F'}{\partial M_x} = - \frac{1}{2t_f} w_{,xx}$$

$$\frac{\partial F'}{\partial M_y} = - \frac{1}{2t_f} w_{,yy} \tag{71}$$

$$\frac{\partial F'}{\partial M_{xy}} = + \frac{1}{t_f} w_{,xy}$$

Midsurface equilibrium equations are

$$\sigma'_{x,x} + \tau'_{xy,y} = 0$$

$$\tau_{xy,x} + \sigma'_{y,y} = 0 \tag{72}$$

In view of equation (72), the lateral equilibrium equation is

$$\sigma'_x (w_{,xx} + w_{o,xx}) + \sigma'_y (w_{,yy} + w_{o,yy}) + 2 \tau'_{xy} (w_{,xy} + w_{o,xy})$$

$$+ \frac{\sigma'_y}{R} + \frac{1}{2t_f} (M_{xx,x} + M_{y,yy} - 2 M_{xy,xy}) = 0 \tag{73}$$

The midsurface stress-displacement boundary integrals are

$$\int_0^{2\pi R} \sigma'_x \, \delta u \Big|_0^L dy = 0 \tag{74a}$$

$$\int_0^{2\pi R} \tau'_{xy} \, \delta v \Big|_0^L dy = 0 \tag{74b}$$

$$\int_0^{L} \sigma'_y \, \delta v \Big|_0^{2\pi R} dx = 0 \tag{74c}$$

$$\int_0^{L} \tau'_{xy} \, \delta u \Big|_0^{2\pi R} dx = 0 \tag{74d}$$

The remaining boundary integrals are

$$\int_0^{2\pi R} \left\{ \sigma'_x \, (w_{,x} + w_{o,x}) + \tau'_{xy} \, (w_{,y} + w_{o,y}) + \frac{1}{2t_f} M_{x,x} - \frac{1}{t_f} M_{xy,y} \right\} \delta w \Big|_0^L dy = 0 \tag{75a}$$

$$\int_0^{L} \left\{ \sigma'_x \, (w_{,y} + w_{o,y}) + \tau'_{xy} \, (w_{,x} + w_{o,x}) + \frac{1}{2t_f} M_{y,y} - \frac{1}{t_f} M_{xy,x} \right\} \delta w \Big|_0^{2\pi R} dx = 0 \tag{75b}$$

$$2 \, M_{xy} \, \delta w \Big|_0^L \Big|_0^{2\pi R} = 0 \tag{75c}$$

The boundary integrals at $x = 0, L$ either vanish because the end shortening is prescribed or can be ignored due to the very large L/R ratio assumed for the orthotropic, two-element cylinder. The boundary conditions at $y = 0, 2\pi R$ are either continuity conditions or conditions which preclude any resultant shear or circumferential load along any generator after subsequent integration over the shell length.

APPENDIX III

METHOD OF SOLUTION FOR THE ELASTIC, ISOTROPIC SANDWICH, CIRCULAR CYLINDRICAL SHELL

Substitution of expressions for the displacements [equations (13), (14), (15), and (16)], stresses [equations (17), (18), and (19)], and transverse shear strains [equations (23), and (24)] into the Reissner functional given by equation (26), and subsequent integration of the result, yields

$$\bar{\Gamma} = \frac{\Gamma^{*}}{2\pi R^{2}\left(\frac{L+2h}{4}\right)} = \frac{1}{E}\Big[F_{33} - A_{32}F_{32} - A_{11}(F_{11} + E_{11})$$

$$- A_{22}(E_{22} + E_{22}) - A_{31}(F_{31} + E_{31})$$

$$- A_{13}(F_{13} + E_{13}) - A_{25}E_{20}$$

$$- \left(\frac{h}{R}\right)^{2}\Big[\frac{1}{2}(A_{11}^{2} + A_{22}^{2})(1 + \lambda_{1}^{2}) + A_{13}^{2}(1 + \lambda_{2}^{2})$$

$$+ A_{31}^{2}(1 + \lambda_{3}^{2}) + 2(A_{32}^{2} + \lambda_{32}^{2})\Big]$$

$$+ \frac{\pi(h/R)}{8(1-\nu^{2})}\Big\{\frac{1}{3}\left(\frac{h}{R}\right)^{2}\Big[(1+\nu)^{2}\xi_{1}^{2} + 2(1-\nu^{2})\xi_{2}^{2} + \xi_{3}^{2}\Big]$$

$$+ \Big[\lambda_{1}^{2}\chi_{11} + 2\lambda_{1}^{2}\chi_{20} + \lambda_{1}^{2}\gamma_{11} + 2\lambda_{1}^{2}\gamma_{02} + 2\lambda_{1}^{2}\chi_{11}\gamma_{11}$$

$$+ \frac{1}{2}\lambda_{1}^{2}\chi_{11}^{2} + \lambda_{1}^{2}\chi_{11}\gamma_{11} + \frac{1}{2}\lambda_{1}^{2}\gamma_{11}^{2} - \nu\left(\frac{1}{2}\lambda_{1}^{2}\chi_{11} + \frac{1}{2}\lambda_{1}^{2}\gamma_{11}\right)\Big]$$

$$+ \sqrt{\frac{1-\nu}{2}}\Big[2\lambda_{1}^{3}\xi_{1}\chi_{11} + 2\lambda_{1}^{3}\xi_{2}\chi_{20} + 2\xi_{1}\lambda_{1}^{2}\gamma_{11}$$

$$+ 2\lambda_{1}^{3}\xi_{3}\gamma_{02} + 2\lambda_{1}^{2}\xi_{1}\chi_{11} + 2\lambda_{1}^{2}\xi_{1}\gamma_{11}\Big]\Big\} + \frac{1}{4}\frac{C_{c}^{2}c}{Et_{f}}\Big[\lambda_{1}^{2}\chi_{11}$$

$$+ \frac{2}{F_{11}} + 2\left(\frac{2}{x_{20}} + \frac{2}{y_{02}}\right)\Bigg] + 4\left(\frac{\dot{\omega}}{\omega}\right)^2 \tag{76}$$

where the F's and E's are defined as

$$F_{00} = -\frac{2}{3}\frac{h}{\omega}\left[\frac{\dot{s}_{11}^2}{8} + \dot{s}_{20}^2 - 2\dot{s}_{11_0}\left(\frac{\dot{s}_{11}}{8} + \frac{\dot{s}_{20}}{4}\right)\right]$$

$$F_{02} = -\frac{2}{3}\frac{h}{\omega}\left[\dot{s}_{11}^2 + 2\dot{s}_{11_0}\dot{s}_{11}\right]$$

$$F_{11} = -\frac{2}{3}\frac{h}{\omega}\left[2\dot{s}_{11}\dot{s}_{20} + \dot{s}_{11}\dot{s}_{02} + 2\dot{s}_{11_0}\left(\dot{s}_{21} + \frac{\dot{s}_{02}}{2} + \frac{\dot{s}_{11}}{4}\right)\right]$$

$$F_{22} = -\frac{2}{3}\frac{h}{\omega}\left[\frac{\dot{s}_{11}^2}{8} + 4\dot{s}_{20}\dot{s}_{02} + 2\dot{s}_{11_0}\left(\frac{\dot{s}_{11}}{8} - \frac{\dot{s}_{02}}{2}\right)\right]$$

$$F_{31} = -\frac{2}{3}\frac{h}{\omega}\left[\frac{2}{3}\dot{s}_{11}\dot{s}_{21} + 2\dot{s}_{11_0}\left(\frac{\dot{s}_{21}}{3} + \frac{\dot{s}_{11}}{12}\right)\right]$$

$$F_{13} = -\frac{2}{3}\frac{h}{\omega}\left[\dot{s}_{11}\dot{s}_{02} + \dot{s}_{11_0}\dot{s}_{02}\right] \tag{77}$$

$$E_{21} = -\frac{2}{3}\frac{h}{\omega}\left[\frac{\dot{s}_{11}^2}{8} + \dot{s}_{11_0}\frac{\dot{s}_{11}}{4}\right] - \frac{2}{3}\frac{h}{\omega}\dot{s}_{21}$$

$$E_{11} = -\frac{2}{3}\frac{h}{\omega}\left[\dot{s}_{11}\dot{s}_{02} + \dot{s}_{11_0}\dot{s}_{02}\right] - \frac{2}{3}\frac{h}{\omega}\dot{s}_{11}$$

$$E_{22} = -\frac{2}{3}\frac{h}{\omega}\left[-\frac{\dot{s}_{11}^4}{8} - \dot{s}_{11_0}\frac{\dot{s}_{11}}{4}\right]$$

$$E_{31} = 0$$

$$E_{13} = -\frac{2}{3}\frac{h}{\omega}\left[-\dot{s}_{11}\dot{s}_{02} - \dot{s}_{11_0}\dot{s}_{02}\right] \tag{78}$$

The substitution of $\epsilon_{21_0} = (\epsilon_{11_0})/4$ has been made above based on the postbuckling analysis results presented in reference 21. The same assumptive was utilized in reference 4 in conjunction with the maximum-strength analysis of initially imperfect cylindrical shells in axial compression, and in reference 22 in conjunction with an elastic analysis of the buckling process for compressed cylinders.

The equations found from the vanishing of the first variation of equation (7) are reduced to four equations in the unknowns ϵ_{11}, ϵ_{21}, ϵ_{12}, and $\bar{r}/R$. For given values of the parameters $\bar{\delta}$, $\bar{\epsilon}$, and $C_c t_c/Et$, a relationship between $\frac{\bar{\sigma}}{\sigma_b}$ and $\frac{e\bar{i}}{t}$ is obtained and plotted in figure 3.

APPENDIX IV

CORRELATION OF THE STIFFNESS PARAMETERS OF THE ORTHOTROPIC TWO-ELEMENT MODEL TO THOSE OF A STIFFENED CIRCULAR CYLINDRICAL SHELL

The classical buckling stress derived in reference 23 for an axially compressed, ring- and stringer-stiffened, circular cylindrical shell is

$$\sigma_{cl_{ST}} = \frac{D}{\bar{t}}\left(\frac{\pi}{\bar{L}}\right)^2 \left\{\left(1+\beta^2\right)^2 + \frac{E_s I_s}{dD} + \beta^4 \frac{E_r I_r}{\ell D} + \left(\frac{G_s J_s}{dD} + \frac{G_r J_r}{\ell D}\right)\beta^2\right\} + \frac{12\bar{Z}^2 D}{\bar{t}\pi^2 \bar{L}^2}\left\{\frac{1 + \bar{S}\bar{\Delta}_s + \bar{R}\bar{\Delta}_r + \bar{S}\,\bar{R}\bar{\Delta}_{rs}}{\bar{\Delta}}\right\} \tag{79}$$

where

$$\bar{\Delta}_r = 1 - 2\alpha^2\beta^2\left(1 - \beta^2\nu\right)\frac{\bar{z}_r}{R} + \alpha^4\beta^4\left(1+\beta^2\right)2\left(\frac{\bar{z}_r}{R}\right)^2$$

$$\bar{\Delta}_s = 1 - 2\alpha^2\left(\beta^2 - \nu\right)\frac{\bar{z}_s}{R} + \alpha^4\left(1+\beta^2\right)\left(\frac{\bar{z}_s}{R}\right)^2$$

$$\bar{\Delta}_{rs} = 1 - \nu^2 - 2\alpha^2\beta^2\left(1-\nu^2\right)\left(\frac{\bar{z}_s}{R} + \frac{\bar{z}_r}{R}\right) + \alpha^4\beta^4\left[1 - \nu^2 + 2\beta^2\left(1+\nu\right)\right]\left(\frac{\bar{z}_r}{R}\right)^2 + 2\alpha^4\beta^4\left(1+\nu\right)^2\frac{\bar{z}_r\bar{z}_s}{R^2} + \alpha^4\beta^2\left[2\left(1+\nu\right) + \beta^2\left(1-\nu^2\right)\right]\left(\frac{\bar{z}_s}{R}\right)^2$$

$$\bar{\Delta} = \left(1+\beta^2\right)^2 + 2\beta^2\left(1+\nu\right)\left(\bar{R}+\bar{S}\right) + \left(1-\nu^2\right)\left[\bar{S} + 2\beta^2\bar{R}\,\bar{S}\left(1+\nu\right) + \beta^4\bar{R}\right] \tag{80}$$

$$Z^2 = \frac{L^4(1 - \nu^2)}{R^2 t^2}$$

$$D = \frac{Et^3}{12(1 - \nu^2)}$$

$$\bar{S} = \frac{E_s A_s}{Etd}$$

$$\bar{R} = \frac{E_r A_r}{Et\ell} \tag{81}$$

$$\alpha = \frac{m\pi R}{L}$$

$$\beta = \frac{nL}{m\pi R}$$

The subscripts s and r refer to properties of the stringers and rings, respectively. The signs preceding the terms linear in $\bar{z}_s$ and $\bar{z}_r$ (distance from the middle surface of the shell to the centroid of the stiffener) have been changed from positive to negative, due to the fact that the z coordinate in reference 23 is measured positive outward, whereas in the present study, z is measured positive inward.

The classical buckling stress of the orthotropic, two-element model is

$$\sigma_{cl_{TE}} = \frac{1}{2t_f}\left(\frac{m\pi}{L}\right)^2 \left\{ \frac{D_x}{1 - \nu_x\nu_y} + \left[\frac{\nu_y D_x + \nu_x D_y}{1 - \nu_x\nu_y} + 2D_{xy}\right]\beta^2 + \frac{D_y}{1 - \nu_x\nu_y}\right\}\beta^4 + \frac{E_x E_y / 2t_f}{\left(\frac{m\pi}{L}\right)^2 R^2 \left[E_x - \left(\mu_y E_x + \mu_x E_y - \frac{E_x E_y}{G_{xy}}\right)\beta^2 + E_y\beta^4\right]} \tag{82}$$

This equation is the same as that derived by Stein and Mayers[24] when the transverse shear stiffness is infinitely large.

To find expressions relating the bending and midsurface stiffnesses of the orthotropic, two-element model to those of the ring- and stringer-

stiffened shell, equations (79) and (82) are equated. For $\bar{z}_s = \bar{z}_r = 0$, the coefficients of like powers of β are required to vanish, thereby leading to the relationships

$$\frac{D_x/2t_f}{1 - \nu_x\nu_y} = \frac{D}{\bar{t}}\left[1 + \frac{E_s I_s}{dD}\right]$$

$$\frac{D_y/2t_f}{1 - \nu_x\nu_y} = \frac{D}{\bar{t}}\left[1 + \frac{E_r I_r}{\ell D}\right]$$

$$D_{xy}/2t_f = \frac{D}{\bar{t}}\left[1 - \frac{\nu_x}{2} - \frac{\nu_y}{2} + \frac{1}{2}\left(\frac{G_s J_s}{dD} + \frac{G_r J_r}{\ell D}\right) - \frac{1}{2}\left(\nu_y \frac{E_s I_s}{dD} + \nu_x \frac{E_r I_r}{\ell D}\right)\right] \tag{83}$$

$$\frac{E_x}{2t_f E} = \frac{k_1}{k_4} = s'_x$$

$$\frac{E_y}{2t_f E} = \frac{k_1}{k_2} = s'_y$$

$$\frac{G_{xy}}{2t_f E} = \frac{k_1}{k_3 + \mu_y k_2 + \mu_x k_4} = \frac{s'_{xy}}{3} \tag{84}$$

where

$$k_1 = \frac{t}{\bar{t}}\left[1 + \bar{S} + \bar{R} + \bar{S}\,\bar{R}\left(1 - \nu^2\right)\right]$$

$$k_2 = 1 + \left(1 - \nu^2\right)\bar{S}$$

$$k_3 = 2\left[1 + \left(1 + \nu\right)\left(\bar{R} + \bar{S}\right) + \left(\bar{R}\,\bar{S}\right)\left(1 - \nu^2\right)\left(1 + \nu\right)\right]$$

$$k_4 = 1 + \left(1 - \nu^2\right)\bar{R} \tag{85}$$

Stiffener eccentricity effects introduce a coupling between extension and bending, as represented by the terms containing $\bar{z}_s$ and $\bar{z}_r$ in equations (80). However, since the orthotropic, two-element model does not contain a corresponding set of coupling terms, stiffener eccentricity effects are included by modifying the bending stiffnesses D_x, D_y, and D_{xy} as follows:

$$\frac{D_x/2t_f}{1 - \nu_x\nu_y} = \frac{Et^3}{12\bar{t}(1 - \nu^2)} \left[1 + \frac{E_s I_s}{dD}\right] - C \frac{\bar{S}t^2 E\left(\frac{t}{\bar{t}}\right)}{1 + (1 - \nu^2)\bar{S}} \left(\frac{\bar{z}_s}{R}\right)$$

$$\frac{D_y/2t_f}{1 - \nu_x\nu_y} = \frac{Et^3}{12\bar{t}(1 - \nu^2)} \left[1 + \frac{E_r I_r}{\ell D}\right] - C \frac{\bar{R}t^2 E\left(\frac{t}{\bar{t}}\right)}{1 + (1 - \nu^2)\bar{R}} \left(\frac{\bar{z}_r}{R}\right)$$

$$\begin{aligned} D_{xy}/2t_f = \frac{Et^3}{12\bar{t}(1 - \nu^2)} & \left[1 - \frac{\nu_x}{2} - \frac{\nu_y}{2} + \frac{1}{2}\left(\frac{G_s J_s}{dD} + \frac{G_r J_r}{\ell D}\right)\right. \\ & \left. - \frac{1}{2}\left(\nu_y \frac{E_s I_s}{dD} + \nu_x \frac{E_r I_r}{\ell D}\right)\right] + \frac{\nu_y}{2}\left[\frac{C\bar{S}t^2 E\left(\frac{t}{\bar{t}}\right)}{1 + (1 - \nu^2)\bar{S}}\left(\frac{\bar{z}_s}{R}\right)\right] \\ & + \frac{\nu_x}{2}\left[\frac{C\bar{R}t^2 E\left(\frac{t}{\bar{t}}\right)}{1 + (1 - \nu^2)\bar{R}}\left(\frac{\bar{z}_r}{R}\right)\right] \\ & - \frac{1}{2}\left[\frac{C(1 - \nu^2)\bar{R}\,\bar{S}t^2 E\left(\frac{t}{\bar{t}}\right)}{2 + 2(1 + \nu)(\bar{R} + \bar{S}) + 2\bar{R}\,\bar{S}(1 - \nu^2)(1 + \nu)}\left(\frac{\bar{z}_s}{R} + \frac{\bar{z}_s}{R}\right)\right] \end{aligned} \tag{86}$$

where C is a nondimensional eccentricity constant.

APPENDIX V

METHOD OF SOLUTION FOR THE ELASTIC, ECCENTRICALLY STIFFENED, CIRCULAR CYLINDRICAL SHELL

Substitution of expressions for the displacements [equations (14), (15), (40), and (41)] and stresses [equations (17), (18), and (19)] into the Reissner functional given by equation (43), and subsequent integration of the result, yields

$$\begin{aligned}
\bar{U} = \frac{U''}{2t_f E\left(\frac{2\pi RL}{4}\right)} = &- 4\frac{\bar{\sigma}}{E}F_{00} - A_{02}F_{02} - A_{11}\left(F_{11} + H_{11}\right) \\
&- 4A_{22}\left(F_{22} + H_{22}\right) - 3A_{31}\left(F_{31} + 3H_{31}\right) + 4\left(\frac{\bar{\sigma}}{E}\right)e \\
&- A_{13}\left(3F_{13} + H_{13}\right) - 8A_{20}H_{20} - \frac{2}{s'_x}\left(\frac{\bar{\sigma}}{E}\right)^2 \\
&- \frac{1}{2}\left\{\left[\frac{1}{s'_x} - \frac{\mu^2}{s'} + \frac{\mu^4}{s'_y} + \frac{3\mu^2}{s'_{xy}}\right]\left(A_{11}^2 + 16A_{22}^2\right)\right. \\
&+ A_{13}^2\left[\frac{81}{s'_x} - \frac{9\mu^2}{s'} + \frac{\mu^4}{s'_y} + \frac{27\mu^2}{s'_{xy}}\right] + A_{31}^2\left[\frac{1}{s'_x} - \frac{9\mu^2}{s'} + \frac{81\mu^4}{s'_y} + \frac{27\mu^2}{s'_{xy}}\right] \\
&\left. + 32\left[\frac{A_{02}^2}{s'_x} + \mu^4\frac{A_{20}^2}{s'_y}\right]\right\} + \frac{\bar{\pi}^2(\bar{t}/R)^2}{8\left(1 - \nu_x\nu_y\right)}\left\{\left(\frac{h_x}{\bar{t}}\right)^2\mu^4\left(\xi_{11}^2 + 32\xi_{20}^2\right)\right. \\
&+ \left(\frac{h_y}{\bar{t}}\right)^2\left(\xi_{11}^2 + 32\xi_{02}^2\right) + \left[\nu_y\left(\frac{h_x}{\bar{t}}\right)^2 + \nu_x\left(\frac{h_y}{\bar{t}}\right)^2\right]\mu^2\xi_{11}^2 \\
&\left. + \frac{2\left(1 - \nu_x\nu_y\right)}{\left(1 + \frac{\nu_x}{2} + \frac{\nu_y}{2}\right)}\left(\frac{h_{xy}}{\bar{t}}\right)^2\mu^2\xi_{11}^2\right\}
\end{aligned} \tag{87}$$

where

$$s' = \frac{s'_x\, s'_y}{\mu_x s'_y + \mu_y s'_x} \tag{88}$$

The midsurface stiffness parameters s'_x, s'_y, and s'_{xy} are, in turn, related to their stiffened circular cylindrical shell counterparts in equations (84) and (85) of Appendix IV, and are repeated here in combined form as

$$s'_x = \frac{\left(\frac{t}{\bar{t}}\right)\left[1 + \bar{S} + \bar{R} + \bar{S}\,\bar{R}(1 - \nu^2)\right]}{1 + (1 - \nu^2)\bar{R}}$$

$$s'_y = \frac{\left(\frac{t}{\bar{t}}\right)\left[1 + \bar{S} + \bar{R} + \bar{S}\,\bar{R}(1 - \nu^2)\right]}{1 + (1 - \nu^2)\bar{S}} \qquad (89)$$

$$s'_{xy} = \frac{3\left(\frac{t}{\bar{t}}\right)\left[1 + \bar{S} + \bar{R} + \bar{S}\,\bar{R}(1 - \nu^2)\right]}{2\left[1 + (1+\nu)(\bar{R}+\bar{S}) + \bar{R}\,\bar{S}(1-\nu^2)(1+\nu)\right] + \mu_y + \mu_x + (1-\nu^2)(\mu_y\bar{S} + \mu_x\bar{R})}$$

The bending stiffness parameters have been presented in equation (39) of the text and are listed here again as

$$\left(\frac{h_x}{\bar{t}}\right)^2 = \frac{1}{3}\left(\frac{1 - \nu_x\nu_y}{1 - \nu^2}\right)\left(\frac{t}{\bar{t}}\right)^3\left[1 + \frac{E_s I_s}{dD}\right] - C\frac{4\bar{S}(1 - \nu_x\nu_y)}{1 + (1 - \nu^2)\bar{S}}\left(\frac{t}{\bar{t}}\right)^3\left(\frac{\bar{z}_s}{R}\right)$$

$$\left(\frac{h_y}{\bar{t}}\right)^2 = \frac{1}{3}\left(\frac{1 - \nu_x\nu_y}{1 - \nu^2}\right)\left(\frac{t}{\bar{t}}\right)^3\left[1 + \frac{E_r I_r}{\ell D}\right] - C\frac{4\bar{R}(1 - \nu_x\nu_y)}{1 + (1 - \nu^2)\bar{R}}\left(\frac{t}{\bar{t}}\right)^3\left(\frac{\bar{z}_r}{R}\right)$$

$$\left(\frac{h_{xy}}{\bar{t}}\right) = \frac{1}{3}\left(\frac{1 + \frac{\nu_x}{2} + \frac{\nu_y}{2}}{1 - \nu^2}\right)\left(\frac{t}{\bar{t}}\right)^3\left[1 - \frac{\nu_x}{2} - \frac{\nu_y}{2} + \frac{1}{2}\left(\frac{G_s J_s}{dD} + \frac{G_r J_r}{\ell D}\right)\right.$$

$$\left. - \frac{1}{2}\left(\nu_y\frac{E_s I_s}{dD} + \nu_x\frac{E_r I_r}{\ell D}\right)\right] + 2\nu_y\left(1 + \frac{\nu_x}{2}\right.$$

$$+ \frac{\nu_y}{2}\left[\frac{C\bar{S}}{1 + (1 - \nu^2)\bar{S}} \left(\frac{t}{\bar{t}}\right)^3 \left(\frac{\bar{z}_s}{R} \right)\right] + 2\nu_x \left(1 + \frac{\nu_x}{2}\right.$$

$$+ \frac{\nu_y}{2}\left) \left[\frac{C\bar{R}}{1 + (1 - \nu^2)\bar{R}} \left(\frac{t}{\bar{t}}\right)\left(\frac{\bar{z}_r}{R}\right)\right] - 2\left(1 + \frac{\nu_x}{2}\right.\right.$$

$$+ \frac{\nu_y}{2}\left) \left[\frac{C(1 - \nu^2)\bar{R}\,\bar{S}\left(\frac{t}{\bar{t}}\right)^3}{2 + 2(1 + \nu)(\bar{R} + \bar{S}) + 2\bar{R}\,\bar{S}(1 - \nu^2)(1 + \nu)} \left(\frac{\bar{z}_r}{R} + \frac{\bar{z}_s}{R}\right)\right] \tag{90}$$

The quantities F_{ij} and H_{ij}, defined in Appendix III, can be used here if h and η are replaced by $\bar{t}$ and $\bar{\eta}$, respectively.

The equations resulting from the vanishing of the first variation of equation (87) with respect to the free coefficients of the assumed stress and displacement functions (equations 13-19) are reduced to four equations in the four unknowns ξ_{11}, ξ_{20}, ξ_{02}, and σ/E. For prescribed values Δ, μ, $\bar{\eta}$, and the stiffened shell parameters, a relationship between $\frac{\sigma R}{E\bar{t}}$ and $\frac{eR}{\bar{t}}$ is obtained and plotted in Figure 5 for eccentrically stiffened, circular cylindrical shells.

UNCLASSIFIED

DOCUMENT CONTROL DATA - R & D

(Security classification of title, body of abstract and indexing annotation must be entered when the overall report is classified)

Stanford University
Department of Aeronautics and Astronautics
Stanford, California

2a. REPORT SECURITY CLASSIFICATION: UNCLASSIFIED

2b. GROUP: N/A

FAILURE ANALYSIS OF INITIALLY IMPERFECT, AXIALLY COMPRESSED, ORTHOTROPIC, SANDWICH AND ECCENTRICALLY STIFFENED, CIRCULAR CYLINDRICAL SHELLS

Type of report and inclusive dates

Final Technical Report

Author(s) (First name, middle initial, last name)

Donald L. Wesenberg
Jean Mayers

6. REPORT DATE	7a. TOTAL NO. OF PAGES	7b. NO. OF REFS
December 1969	76	27

8a. CONTRACT OR GRANT NO.	9a. ORIGINATOR'S REPORT NUMBER(S)
DAAJ02-68-C-0035 Task 1F162204A17002	USAAVLABS Technical Report 69-86
	9b. OTHER REPORT NO(S) (Any other numbers that may be assigned this report)

This document is subject to special export controls, and each transmittal to foreign governments or foreign nationals may be made only with prior approval of US Army Aviation Materiel Laboratories, Fort Eustis, Virginia 23604.

	12. SPONSORING MILITARY ACTIVITY
	U.S. Army Aviation Materiel Laboratories Fort Eustis, Virginia

The maximum strength analysis of initially imperfect, axially compressed, orthotropic, sandwich and eccentrically stiffened, circular cylindrical shells has been developed through the use of Reissner's variational principle, von Kármán-Donnell kinematics, and a deformation theory of plasticity. For a given material and for the special cases of isotropic sandwich cylinders and conventional cylinders with eccentrically located longitudinal stiffeners, the results of the analysis reflect significant reductions in load-carrying capability in the range of "effective" radius-to-thickness ratios of practical interest.

DD FORM 1473

UNCLASSIFIED

Security Classification

Shell Structures
Stability
Maximum Strength
Failure Analysis
Plasticity
Stiffened and Sandwich Construction
Stiffener Eccentricity Effects